Composition and chemical processing of volatile organic compounds in boundary layer polluted plumes: Insights from an airborne Q-PTR-MS on-board the French ATR-42 aircraft

Pamela Dominutti, Baye T. P. Thera, Aurélie Colomb, Agnès Borbon

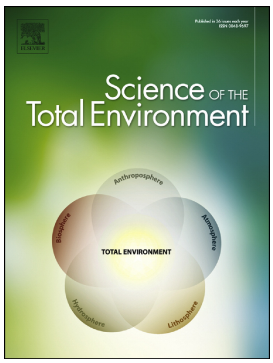

Composition and chemical processing of volatile organic compounds in boundary layer polluted plumes: Insights from an airborne Q-PTR-MS on-board the French ATR-42 aircraft

Pamela A. Dominutti, Baye T.P. Thera, Aurélie Colomb, Agnès Borbon

PII: S0048-9697(24)03458-2

DOI: https://doi.org/10.1016/j.scitotenv.2024.173311

Reference: STOTEN 173311

To appear in: *Science of the Total Environment*

Received date: 6 December 2023

Revised date: 16 April 2024

Accepted date: 15 May 2024

Please cite this article as: P.A. Dominutti, B.T.P. Thera, A. Colomb, et al., Composition and chemical processing of volatile organic compounds in boundary layer polluted plumes: Insights from an airborne Q-PTR-MS on-board the French ATR-42 aircraft, *Science of the Total Environment* (2023), https://doi.org/10.1016/j.scitotenv.2024.173311

Composition and chemical processing of Volatile organic compounds in boundary layer polluted plumes: insights from an airborne Q-PTR-MS on-board the French ATR-42 aircraft.

Pamela A. Dominutti[1,2], Baye T.P. Thera[1§], Aurélie Colomb[1], Agnès Borbon[1*]

[1] Université Clermont Auvergne, CNRS, Laboratoire de Météorologie Physique (LaMP), F-63000 Clemont-Ferrand, France

[2] Université Grenoble Alpes, CNRS, IRD, INP-G, IGE (UMR 5001), Institut des Géosciences de l'Environnement (IGE), 38000, Grenoble, France

[§] TNO, Environmental Modelling, Sensing and Analysis, Petten, the Netherlands

* Corresponding author: agnes.borbon@uca.fr

Abstract

Over the last decade, the French ATR-42 research aircraft explored contrasting polluted plumes in the Paris megacity, the North-West Mediterranean Basin (WMB) and South West Africa (SWA) in the framework of the MEGAPOLI, ChArMEx/SAFMED and DACCIWA international projects, respectively. Major VOCs were measured by a high-sensitivity airborne Quadrupole Proton Transfer Reaction Mass Spectrometer (Q-PTR-MS), showing a robust and consistent response.

Regardless of the location, the air mass composition is dominated by oxygenated VOC (OVOC: methanol, formaldehyde, acetaldehyde, acetone and isoprene oxidation products), which explain 70% of the total VOC burden measured by the Q-PTR-MS. The distribution between OVOC, anthropogenic AVOC and biogenic BVOC is consistent between the three regions. The calculated OH loss rates (12 s^{-1}) and ozone-forming potential (1200 OFP-relative ppb) are three times higher in the SWA plumes. These values are consistent with the

calculated and measured reactivities at the ground. The reactivity of the plumes is by far dominated by biogenic BVOC.

The chemical processing of VOC was examined by establishing various metrics linking Δ[O/VOC] (VOC or oxygenated VOC), plume dilution and the time processing of the plume (cumulative OH exposure Δt[OH] and the linear decay of primary AVOC and the production/decay of secondary OVOC). As expected, Δ[Ox]/Δ[CO] increases with Δt[OH], with significant R^2 (0.58 to 0.93). AVOC (aromatics) usually show a decay rate between -0.5 and -3.2 ppt_{AVOC} ppb_{CO}^{-1} per hour, while OVOC either show an increase (secondary production) or a decrease. The production rate is by far the strongest, up to 18 ppt_{OVOC} ppb_{CO}^{-1} per hour (acetaldehyde) during the eastern flight 33 in Paris. Our results set a benchmark for future photochemical studies to compare with. While the anthropogenic origin of some BVOC (terpenoids) and interferences are not excluded, it also emphasizes the importance of the VOC biogenic fraction in anthropogenically influenced environments, which is expected to increase in a warming climate.

Keywords: MEGAPOLI; CHARMEX; DACCIWA; Air pollution; oxidative capacity; VOC

1. Introduction

Atmospheric pollution is the largest environmental risk for health, causing about 7 million human deaths per year (WHO, 2018). On a global scale, large urban centers are major contributors to air pollution and present a major challenge for the environment and public health (La Colla et al., 2021; Molina, 2021; Vohra et al., 2022). The population growth in those areas affects the energy demand, transportation and industrial activities, which in turn lead to poor air quality. More than 40% of the global population resides in tropical megacities, which are expected to surpass 50% by 2050 mainly in the Africa and Asia regions

(Hoornweg and Pope, 2017). This has the potential for severe impacts on air quality and climate, as megacities represent an overwhelming contribution to air pollutant emissions (Duren and Miller, 2012; Vohra et al., 2022). The increasing urbanization not only affects air quality, regional climate and ecosystems within urban areas but also downwind of these regions (Kanakidou et al., 2011). This phenomenon arises from both locally produced atmospheric pollutants and from those transported in various space-time scales, mainly associated to the transformation of primary emissions. The primary pollutants emitted from urban areas are influenced by solar radiation and atmospheric transport, which leads to their transformation into secondary pollutants.

Despite the efforts in the last years to improve air quality in urban areas, the enlargement of the megacities and their population growth have not eliminated the air pollution problem but in some megacities, it has strengthened (Varotsos et al., 2021).

Among atmospheric pollutants, volatile organic compounds (VOCs) are among the principal trace constituents in the atmosphere and include non-methane hydrocarbons (NHMHCs), oxygenated VOC (OVOC), and other organic compounds (Watson et al., 2001). VOCs have impacts on the formation of secondary pollutants, such as tropospheric ozone and secondary organic aerosol (SOA). They have both natural and anthropogenic primary sources. Natural emissions, mainly released by terrestrial vegetation, are the largest source of biogenic VOC (BVOC) emissions on a global scale, accounting for 90% of the total VOCs (Finlayson-Pitts & Pitts, 2000; Guenther, 2000). However, in urban areas, anthropogenic VOCs (AVOC) represent the main fraction of these compounds, emitted by combustion-related sources (vehicular and biomass burning), volatile chemical products like personal care products, fuel production and transport. While traffic has been recognized as the traditional dominant source of VOCs, the activities related to the use of volatile chemical products like domestic ones are emerging as a largely underestimated new source (McDonald et al., 2018).

It is, therefore, important to quantify their atmospheric abundance and to understand the dynamics of their sources and sinks. Several studies have been conducted to analyze the burden and reactivity of VOC species in urban areas to evaluate their effects on the formation of secondary pollutants (Kansal, 2009; Ma et al., 2019; Tan et al., 2018) (Li et al., 2017). Furthermore, there has been a significant increase in the number of aircraft campaigns over the last years, performed to analyze the composition and the reactivity of the VOC burden inside urban plumes (Apel et al., 2010; Borbon et al., 2013; Crawford et al., 2021; Hopkins et al., 2009; Pfister et al., 2017; Ryerson et al., 2013; Simpson et al., 2020; Warneke et al., 2016; Wilde et al., 2021). However, most of these studies were conducted at mid-northern latitudes, focusing on biogenic and urban emissions, fires and gas and oil emissions. There is still a lack of knowledge about the burden and reactivity of VOCs in areas at lower latitudes and under high anthropogenic pressures, such as the Mediterranean Basin and South West Africa.

Here, we report airborne measurements from three international field studies MEGAPOLI (http://megapoli.info), ChArMEX/SAFMED (http://*charmex*.lsce.ipsl.fr) and DACCIWA (https://www.imk-tro.kit.edu/10052.php), conducted in July 2010, 2013 and 2016. Those three regions encompass a diversity of environments in terms of ozone precursor emissions, emission regulations, urbanization and photochemical conditions (Flamant et al., 2018; Freney et al., 2018; Lelieveld et al., 2012; Monks et al., 2009). Measurements of VOC and other reactive trace gases were performed by the French ATR-42 research aircraft of Safire during all campaigns. In a previous paper, Thera et al. (2023) analyzed the oxidative photochemistry in an ozone-NOy perspective within those plumes. The positive dependence of Ox (ozone+NO_2) to NO indicated a VOC-sensitive regime inside the plumes excepted a rural-like chemistry behaviour at moderate NOx levels (NOx-sensitive). In the present paper, we investigate the atmospheric composition and the chemistry of the VOC burden as long as the plume is moving away from emissions. We apply various reactivity metrics to assess the

potential effects of primary and secondary VOCs on the processing of the plumes and ozone formation. Various VOCs were measured by a common high-sensitivity airborne Quadrupole Proton Transfer Mass Spectrometer (Q-PTR-MS) (Borbon et al., 2013). Those measurements provide a unique and comparable VOC dataset in the three contrasting regions.

2. Materials and methods

2.1. Field campaigns

The MEGAPOLI, ChArMEX/SAFMED, and DACCIWA airborne campaigns took place in the summertime during July 2009, 2013, and 2016, respectively. During MEGAPOLI, the Safire ATR-42 was based on the airport of Cergy Pontoise (49.1° N, 2.0° E), and the campaign was developed over the Paris region. During the ChArMEX/SAFMED campaign, the Safire ATR-42 was based at the airport of Genoa (44.4°N, 8.8° E), and research flights were performed in the North-West Mediterranean region (WMB). The DACCIWA aircraft campaign encompassed the Gulf of Guinea and many South West African (SWA) regions, including Ivory Coast, Ghana, Togo, and Benin. Detailed information about MEGAPOLI, ChArMEX/SAFMED and DACCIWA aircraft campaigns can be found in Thera et al. (2022) and references therein. Flights were performed from the ground to an altitude higher than 3000 m with an exploration at various altitude levels. During each flight, at least one vertical sounding was performed to describe the vertical structure of the troposphere and the distribution of the various physicochemical components.

2.2. Instrumentation and VOCs of interest

2.2.1. Proton Transfer Reaction Mass Spectrometer (Q-PTR-MS)

Apart from formaldehyde (see next section), all the VOC species were measured by a high-sensitivity Quadrupole Proton Transfer Reaction Mass Spectrometer (Q-PTR-MS) from Ionicon Analytik (Innsbruck, Austria). This latter was redesigned to fit in the Safire ATR-42.

Details about the Q-PTR-MS configuration and performances during the MEGAPOLI and SAFMED (ChArMEX) campaigns can be found elsewhere (Borbon et al., 2013; Freney et al., 2018). The same instrument was deployed during the three airborne campaigns to measure the concentration of twelve VOC protonated masses during the flights. More details about the m/z and VOCs can be found in the supplement information. In the following, we will preferably use the name of the corresponding VOC rather than the mass m/z. However, as discussed in the supplement information, interferences cannot be excluded and will be discussed. We have separated the species into three groups of VOCs, namely, BVOCS (Biogenic VOCs) of primary and secondary origins, AVOCS (Anthropogenic VOCs), and OVOCs (Oxygenated VOCs), as follows:

BVOC: m/z 69 (isoprene), m/z 71 (MVK+MACR), m/z 73 (MEK) m/z 137 (monoterpenes),

AVOC: m/z 79 (benzene), m/z 93 (toluene), m/z 107 (C_8 aromatics), m/z 121 (C_9 aromatics),

OVOC: m/z 33 (methanol), m/z 42 (acetonitrile), m/z 45 (acetaldehyde), and m/z 59 (acetone).

The instrumental setup developed during DACCIWA is quite similar to the previous ones. VOCs were measured at a time resolution of 20 s, and the Q-PTR-MS drift tube was operated at 2.2 mbar and 60ºC with a drift field of 600 V cm^{-1}. Ambient air was directly pumped by the Q-PTR-MS at a constant flow rate of 75 mL min^{-1} through an inlet directly connected to the instrument. A 4-way valve is installed upstream to sample ambient air, air from the cabin during take-off /landing, or external gases. The background signal was determined through periodic air sampling of ambient air scrubbed through a custom-built catalyst converter (platinum-coated steel wool) heated to 250 °C. Typical background counts for aromatics were between 1.69 and 8.14 counts sec^{-1}, with maximum values observed for oxygenated compounds between 1.96 to 210 counts sec^{-1}.

Detection limits, defined as 3σ of background mixing ratios, ranged from 0.02 to 0.34 ppb_V over a 1s dwell time. Two complete calibrations over a 0.5–8 ppb_v range were performed during each aircraft field campaign at the ground. The standard gas used was provided by Ionimed (Innsbruck, Austria) and contained several VOCs, including benzene, toluene, o-xylene, α-pinene and isoprene at 1 ppm_V certified at ± 5 %. The sensitivity for all major VOCs (the slope of the mixing ratio concerning production signal normalized to H_3O^+) ranged from 3.57 (m/z 137) to 18.8 (m/z 59) counts s^{-1} ppb_v^{-1}. A second 4ppb_v gaseous standard from NPL (UK, University of York) was used to cross-check the quality of the calibration and to perform a calibration control for isoprene and C_6–C_9 aromatics. A relative difference of 10% for isoprene and 16% for aromatics was measured.

The sensitivities of the instrument on the field for eleven masses over the last decade are compared in Figure 1, including the three aircraft campaigns of interest. The sensitivities are consistent between the various ground-based and aircraft campaigns. After 2012, the instrument was optimized, and the sensitivity was improved by almost a factor of 2 for most target protonated masses.

Interferences cannot be excluded in urban environments like recently Coggon et al. (2023) reported for isoprene and urban VOCs in urban environments. During the TRANSEMED campaigns (2011 and 2014 – Figure 1), the aircraft Q-PTR-MS was deployed at ground sites in urban areas of the East Mediterranean and the VOCs were intercompared with co-located GC-FID. Aromatic measurements were consistent at ±20% with an R^2 higher than 0.85 (Thera et al., 2019). The presence of furans in biomass-burning plumes was reported in previous studies (Hornbrook et al., 2011; Warneke et al., 2011). In Paris, furans were measured during the wintertime campaign of the MEGAPOLI experiment by an online GC-FID (Roukos et al., 2009). The levels do not exceed 45±44 ppt_v and represent less than 10% of m/z 69 levels at 431±192 ppt_v. For this study, m/z 69 will be referred to as isoprene.

2.2.2. Formaldehyde measurements

Formaldehyde (HCHO) measurements during DACCIWA and ChArMEX/SAFMED were performed by the Aerolaser AL 4021 instrument. The detection principle is based on the Hantzsch reaction. This technique, often used onboard research aircraft, has already been described in previous studies. The Hantzsch reaction is a specific reaction between an aldehyde, here formaldehyde, and a β-diketone (acetylacetone) in the presence of a nitrogen donor (ammonium acetate in our case) to obtain a fluorescent product, the 3,5-diacetyl-1,4-dihydrolutidine (DDL). The latter is excited at 400 nm by a mercury lamp and emits fluorescent radiation at 510 nm. The quantification of formaldehyde is thus carried out directly by measuring the fluorescence of DDL or its phenyl derivatives at 510 nm (Nash, 1953). In the past, the performance of the instrument was evaluated against other instruments, such as Differential Optical Absorption Spectrometry (DOAS) and Fourier Transfer Infra-Red (FTIR) Interferometry and showed acceptable differences not exceeding 11% (Hak et al., 2005). The resolution of the instrument is 10 s, whereas the detection limit is on the order of 43-50 ppt (Colomb et al., 2006). The precision and accuracy of the instrument are estimated to be on the order of 10% and 20%, respectively (Borbon et al., 2012). It allows measurement of HCHO every 10 s, with a detection limit of 50 ppt_v. No formaldehyde measurements were performed during the MEGAPOLI campaign.

2.2.3. Other instruments onboard the ATR-42

Ozone and carbon monoxide (CO) were sampled through a rear-facing 1⁄4-inch Teflon tube. During MEGAPOLI and SAFMED, ozone and CO were measured using ultraviolet and infrared analyzers (Thermo Fisher environmental instruments) with the MOZART instrument (Nedelec et al., 2003). During DACCIWA, ozone was measured with a commercial analyzer (Thermo Environmental Instrument TEI49i UV photometric), and CO was measured with an analyzer based on cavity ring-down spectroscopy (CRDS) technology developed by

PICARRO Inc. (Filges et al., 2015). During MEGAPOLI and ChArMEX/SAFMED, nitrogen oxides (NO and NO_2) were sampled through a separate rear-facing pressure-controlled inlet at a 30s-time resolution and measured using the MONA (Measurement of Nitrogen on Aircraft) instrument developed by the Laboratoire interuniversitaire des Systèmes Atmosphériques (LISA). MONA consists of three NO commercial analyzers (Ecophysics CLD-780 TR). It measures NOx ($NO+NO_2$) and NOy (sum of NOx and its oxidation products) concentrations by ozone chemiluminescence. NO is directly detected, and NO_2 is converted into NO by a photolytic converter. NOy is converted in NO by a gold converter heated at 200°C with H_2. NOy measurements were performed using a separate heated (60°C) sampling line to avoid any loss of nitric acid. Additional details of the MONA are supplied in the Supplement Material of Freney et al. (2014). During the DACCIWA campaign, nitrogen oxides (NOx) were measured by a TEI42 iTL chemiluminescence detector with a blue light photolytic converter instrument, which converts only NO_2 into NO. The performances are reported by Thera et al. (2022).

2.2.4. Quality control procedures

The quality control procedure included detecting missing and negative values and observations below the method detection limit (MDL). However, it should be noted that the data used in this study was collected from open databases: ETHER for MEGAPOLI (http://cds-espri.ipsl.upmc.fr/megapoli/index.jsp), SEDOO for SAFMED (ChArMEX) (https://mistrals.sedoo.fr/ChArMEx) and DACCIWA (https://baobab.sedoo.fr/DACCIWA) where all the data are validated using a harmonized quality/control procedure such as the one used within the ACTRIS program (Aerosol, Clouds and Trace gases Research Infrastructure, (Hoerger et al., 2015)). Since the data are collected for many species with different resolution times, mean values were calculated for CO, O_3, NO_x, HCHO, and meteorological parameters

to harmonize them with the Q-PTR-MS data. After filtering data, we had to invalidate m/z 69 (isoprene) concentrations from SAFMED (ChArMEX) dataset since it did not meet the quality control procedure.

2.3. Data selection

Figure 2 shows the plot trajectories colour-coded by the mixing ratio of an AVOC (toluene) for the selected flights of this study for each aircraft campaign within the boundary layer. The data selection criteria in this study are the same applied by Thera et al. (2022). The identification of (i) the boundary layer height was performed by the vertical profile of ozone mixing ratios and the relative humidity, and (ii) urban (polluted) plumes in that boundary layer were performed by using NO_x and wind direction to make sure that sampled air masses are located downwind urban areas. In SWA, the type of plume (urban or biomass burning) has also been identified using the ratio of NO_x to CO, according to Denjean et al. (2020). The urban plumes identified in this study were those presenting a ratio greater than 1.

The average height of the boundary layer found in Thera et al. (2022) is used in this study, which is, on average, 2000 m of altitude for Paris, 1000 m for the WMB and 2000 m for SWA. Table 1 shows the summary of the selected flights, the period of flights, the ozone pollution level, the sectors flown, and the average total VOC found inside and outside (background) the plume.

2.4. Metrics

To evaluate and compare the reactivity potential of the plumes between the three aircraft campaigns, we use different metrics based on airborne observations. Those metrics include the ·OH loss rate (kiVOCi), the ozone formation potential (OFP), the primary decay of O/VOC and the secondary production of OVOC and oxidants in the plume. Those metrics

have been temporally constrained by the photochemical age of the air masses, either expressed as the ·OH time exposure (Δt·OH) or the time processing. In the following section, we describe the different metrics.

2.4.1. VOC reactivity

2.4.1.1. The OH loss rate (k_iVOC_i)

During the day, VOCs react mainly with the hydroxyl radical (·OH). The OH loss rate (k_iVOC_i) describes the capacity of the OH consumption by each VOC species (Yu et al., 2020). It is the product of each VOC mixing ratio ($[VOC]_i$) and its OH reaction rate coefficient k_i^{OH}(Wu et al., 2017) according to equation (1):

$$k_iVOC_i = [VOC]_i \times k_i^{OH} \quad (1)$$

where k_iVOC_i is expressed in s^{-1}, $[VOC]_i$ in molecule.cm^{-3} and k_i^{OH} in cm^3 $molecule^{-1}s^{-1}$

For an air mass, the total OH loss rate is expressed as the sum of individual k_iVOC_i calculated from the measured VOC. In this study, the values of k_i^{OH} have been extracted from Seinfeld and Pandis (2006) and reported in Table S1 of the supplement material. The rate constants of the VOC toward ·OH radicals have been calculated (following the formulas in Table S2) for the three contrasting regions given the contrasting climatic conditions and are similar, with some slight discrepancies.

2.4.1.2. The Ozone Formation Potential of VOCs (OFP)

Once VOC oxidation is initiated by the reaction with ·OH in the presence of NO_x, it leads to the photochemical formation of O_3. The Ozone Formation Potential (OFP) represents the ability of each VOC to produce tropospheric ozone and is calculated as follows:

$$OFP\ (VOC)_i = [VOC]_i \times POCP_i \quad (2)$$

where $[VOC]_i$ is the mixing ratio of one VOC and $POCP_i$ is the photochemical ozone creation potential developed by Derwent et al. (2010) and Jenkin et al. (2017). POCP values are usually relative values where the amount of ozone produced from a given VOC is divided by the amount of ozone produced from an equally large emission of ethene (Herndon et al., 2008; Wood et al., 2009) (Table S1). For an air mass, the total OFP is the sum of each OFP (VOC) and is usually used to represent the maximum contribution of VOC species to ozone formation under optimal conditions (Hui et al., 2018; Niu et al., 2016).

2.4.2. The chemical processing of the plume

While the plume ages, one can observe the dilution of atmospheric species and the consumption of primary O/VOC (representing any VOC or oxygenated VOC species) mainly by oxidation with the OH radical during the day or/and secondary production of OVOC (Borbon et al., 2013; Warneke et al., 2007). The oxidation by OH has been previously highlighted in Paris and New York plumes by the decrease of the ratio *m*+*p*-xylenes-to-acetylene and, in parallel, the increase of acetaldehyde-to-acetylene as a function of the photochemical age of the plume (Borbon et al., 2013; Warneke et al., 2007). Acetylene is used as a conservative tracer to take into account the dilution effect. *m*+*p*-xylenes and acetaldehyde are used as primary and secondary VOC, respectively, consumed or produced during plume ageing. The production of oxidants known as O_x (sum of ozone and NO_2) also expresses the secondary production: it quantifies the net photochemical formation of O_3 beyond its rapid daytime interconversion with NO_2. NO_2 is included because it acts as a reservoir of O_3. Therefore, O_x tends to be a more conservative quantity than O_3, not affected by the titration reaction by NO_x (Thera et al., 2022).

The primary O/VOC (representing any VOC or oxygenated VOC species) decay and the secondary production of OVOC and Ox is quantified by $\frac{\Delta[X]}{\Delta[CO]}$ constrained by the processing

time of the plume. Δ is the difference between the mixing ratios of the target species (X) and CO inside the plume and the background values of X and CO (outside the plume). $\Delta[X]$ is divided by CO mixing ratios because the latter is a relatively unreactive tracer of dilution, like acetylene (see above). Dividing by [CO] provides a dilution adjustment similar to the ratio of organic aerosol to CO used in previous studies (Herndon et al., 2008; Kleinman et al., 2008).

- ✓ Calculation of $\frac{\Delta[X]}{\Delta[CO]}$:

The calculation of $\frac{\Delta[X]}{\Delta[CO]}$ follows equation (3):

$$\frac{\Delta[X]}{\Delta[CO]} = \frac{[X]inside\ the\ plume - [X]background}{[CO]inside\ the\ plume - [CO]background} \quad (3)$$

where [X] represents the mixing ratios of OVOC or Ox obtained between inside and outside the plume (background).

- ✓ Constraining the chemical processing of the plume :

The primary O/VOC decay and secondary OVOC production rates from Equation 3 are constrained by the chemical processing of the plume.

The processing time is a first proxy of the plume chemical processing (or ageing), defined by Brito et al. (2018) and adapted by Thera et al. (2022), which is the ratio between the distance from the source area (Paris, Abidjan, Accra and Lomé for this study) by the integrated wind speed along the flight. The processing time does not exceed 10 hours and is usually around 3 hours on average.

Another metric measuring the extent of the chemical processing is the ·OH exposure. The cumulative ·OH exposure, also known as $\Delta t[OH]$, measures the extent of the atmospheric oxidation of emitted VOC (Roberts et al., 1984). It was quantified in previous studies by using the ratios of hydrocarbon species with dissimilar reactivities towards·OH (Herndon et

al., 2008; Roberts et al., 1984; Wood et al., 2009). Usually, C_9-aromatics and benzene species are used to calculate the OH exposure. This is an effective method since C_9 aromatics have relatively short atmospheric lifetimes (3 to 12 hours) in urban areas (Dusanter et al., 2009) compared to that of benzene (9.5 days) (Delmas et al., 2005). Our study observed no progressive decay of the urban peak for aromatics compounds. As an alternative, NO_x and CO have been used according to equation 4 due to the relatively short atmospheric lifetime of NO_x (a few hours, Liu et al., 2016) compared to that of CO (about one or two months) :

$$\Delta t[OH] = \frac{1}{k_{NOx} - k_{CO}} \times \left[ln\left(\frac{[NO_x]}{[CO]}\right)_{to} - ln\left(\frac{[NO_x]}{[CO]}\right)\right] \qquad (4)$$

where the brackets denote the concentrations of the species and k_x is the rate coefficient of the hydroxyl radical reaction with the corresponding species.

$k_{NO} = 3.3 \times 10^{-11}(\frac{T}{300})^{-0.3} cm^3\ molecule^{-1}s^{-1}$ (Fulle et al., 1998)

$k_{NO2} = 7.5 \times 10^{-11} cm^3\ molecule^{-1}s^{-1}$ (Fulle et al., 1998)

$k_{CO} = 1.57 \times 10^{-13} cm^3\ molecule^{-1}s^{-1}$ (McCabe et al., 2001)

$k_{NOx} = \frac{k_{NO}+k_{NO2}}{2}$

t_0 is the time of the first interception of the plumes.

The single use of NO_2 to estimate k_{NOx} is an alternative and was tested on flight 36. The difference inside the plume is lower than 5% and the OH exposure follows the same evolution as long as the plume travels away from Paris centre.

3. Results and discussion

3.1 Meteorological conditions

The meteorological conditions encountered during the MEGAPOLI, SAFMED and DACCIWA aircraft campaigns are described in Thera et al. (2022) and references therein.

The observed spatial gradient in air temperature, humidity and NO_2 photolysis frequencies towards lower latitudes is consistent with the climatic latitudinal gradient. Indeed, the temperature in Paris varies between 11.7 and 22.2 °C and rarely exceeds 20 °C on average, while it varies between 23 to 28 °C in the WMB and from 20 to 24 °C in SWA. Average wind speed ranges between 4.3 and 9.1 m s^{-1} in Paris, while a larger range is observed in SWA (from 3.9 to 11.4 m s^{-1}), and a lower range is observed in the WMB with an average value of 4.5 m s^{-1}. Average relative humidity was the lowest during the MEGAPOLI campaign (54% at maximum) and got higher in the WMB (up to 62 %) and SWA (up to 87 %).

3.2. Overview of VOC and trace gas mixing ratios

Figure 3 reports the average mixing ratio values of each VOC measured inside and outside the plumes and the average total VOC inside the plumes. These values are compared to the ones measured at ground sites. Table 2 summarises the statistical values of the twelve VOC measured by the airborne Q-PTR-MS in the three contrasting regions during the MEGAPOLI, SAFMED and DACCIWA campaigns.

The average total VOC (TVOC) are in the same order in the plumes of the three compared regions. An average TVOC mixing ratio of 11.8 ± 8.5 ppb_v was observed inside the Paris plume, 16.8 ± 13.6 ppb_v were observed inside the plumes in SWA and lower average values, 9.6 ± 5.2 ppb_v, were measured in the WMB area. Regardless of the region, oxygenated VOCs represented the dominant fraction and accounted for at least 64% of TVOC, followed by BVOC (23-26 % of the TVOC) (Figure 3). Aromatic compounds (AVOC) only account for 7-10% of the TVOC inside the plumes of the three regions. Even though isoprene data was invalidated during the SAFMED campaign and formaldehyde was not measured during MEGAPOLI, the same proportion of VOC groups, namely BVOC, AVOC and OVOC, is observed inside the three contrasting areas and is discussed in the next sections.

In addition to the VOC measured by the Q-PTR-MS, formaldehyde has also been measured during DACCIWA and SAFMED campaigns and will be counted among the OVOCs. The TVOC mixing ratio gets higher in SWA with an average of 16.8 ppb_v only considering Q-PTR-MS measurements and goes up to 20.3 ppb_v on average when formaldehyde is added.

BVOC (isoprene, MACR+MVK, MEK and monoterpenes) mixing ratios present the same range in Paris and WMB plumes with average values of 2.74 ± 3.05 and 2.51 ±1.5 ppb_v, respectively (Table 2). Conversely, higher average mixing ratios were observed in SWA plumes (4.21 ± 3.5 ppb_v), which could be related to the overflown surface condition with biogenic emission sources related to forests in SWA areas. Differences in concentrations were also found inside and outside the plumes. BVOC mixing ratios are 1.2 to 1.5 higher outside the Paris plume, where there are more isoprene emitters like tempered forest than inside the plume. Contrarily, except for the total monoterpenes, BVOC mixing ratios are 1.2 to 1.5 higher inside the SWA plume than outside (Figure 3). Dominutti et al. (2019) have detected a significant amount of terpenoids in the exhaust of various combustion sources in Abidjan, including fossil fuels, waste and domestic burning. Therefore, besides the biogenic one, an additional fraction of anthropogenic isoprene and monoterpenes in SWA plumes cannot be excluded.

The mixing ratios of AVOC (sum of benzene, toluene, C_8 and C_9 aromatics) are in the same range in the three contrasting regions with a value of 0.82 ± 0.66 ppb_v inside Paris plume, 1.20 ± 1.10 ppb_v in SWA plume and an average of 1.0 ± 0.8 ppb_v in WMB. Aromatic compounds are in the same range (benzene and C_9 aromatics) or 1.3 times higher inside the Paris plume than outside (toluene and C_8 aromatics). Similarly, they are either in the same range (C_8 and C_9 aromatics) or 1.2 higher (toluene) and lower (benzene) inside the plumes than outside the plumes in SWA (Figure 3).

The sum of average mixing ratios of OVOC (methanol, acetaldehyde, and acetone) was the lowest during SAFMED (6.1 ± 3.0 ppb_v), and they get higher towards lower latitudes inside Paris plumes (8.3 ± 5.7 ppb_v) and SWA urban plumes (14.9 ± 13.8 ppb_v). Additionally, similar mixing ratios of formaldehyde were observed during DACCIWA and SAFMED campaigns, with average values of 3.52 ± 1.97 and 3.60 ± 0.80, respectively (Table 2).

The average mixing of OVOC is 1.3 to 1.7 times higher outside the Paris plume than inside (Figures 3 and 4). This can be due to the production of secondary VOC favoured by the processing time and the primary sources of OVOC (mainly from biogenic sources) favoured by environmental conditions such as temperature and humidity (moisture). The opposite pattern is observed in SWA, where apart from methanol, for which the same mixing ratio is observed inside and outside the plume, there is 1.6 and 1.8 more OVOC inside than outside the plumes. One possible explanation can be the anthropogenic sources of OVOC from urban areas in SWA. The high contribution of OVOCs in urban areas has already been reported in previous studies. Langford et al., have found that OVOCs were the most abundant compounds in London, indicating the importance of primary emissions and photochemistry taking place in this region (Langford et al., 2010). Similarly, Rantala et al., measured VOC fluxes in Finland. They have found a high contribution of methanol regardless of the season and other OVOCs (ethanol, acetone and acetaldehyde), suggesting the contribution from biogenic and anthropogenic sources (Rantala et al., 2016). From measurements performed in Innsbruck and compared with other European sites, Karl and co-authors have shown that urban OVOCs would be at least about a factor of 2.1 higher than projections used in these emission inventories, and they suggest it cannot be explained by photochemical processing alone (Karl et al., 2018).

Average VOC mixing ratios have also been compared to ground-based campaigns in the studied regions. It is found that the average mixing ratios of the VOC measured from two

ground sites (SIRTA and LHVP) in Paris during the MEGAPOLI campaign (Ait-Helal et al., 2014) are in the same range as those found in this study (Figure 3). The average mixing ratios of VOC found in Lagos (Murphy et al., 2010) in the framework of the AMMA aircraft campaign, as well as those found from ground-based measurements in Abidjan during the DACCIWA campaign (Dominutti et al., 2019), were within the same range as those found in SWA in this study. The average mixing ratios of VOC measured in the Ersa site (Cape Corsica) in the WMB (Debevec et al., 2021) are also in the same range as those measured during the SAFMED aircraft campaign.

Higher mixing ratios of toluene and C_8-aromatics were observed in ground-based measurements in Abidjan and LHPV, Paris, than those from airborne measurements. This difference could be related to the distance to emission sources, the dilution and the reactivity of both aromatic compounds, affecting their lifetime and atmospheric concentrations.

Globally, a good consistency between airborne and ground-based measurements is observed, which enables the evaluation of the chemical processing of VOC in the atmosphere and the assessment of emission sources in these three contrasted regions.

3.3. Photochemistry of VOCs

3.3.1. Atmospheric reactivities of measured VOC

Figure 4 depicts mean concentrations and the standard deviations, of the OFP and kiVOCi reactivity for BVOC, AVOC and OVOC inside and outside the plumes. The kiVOCi reactivity and ozone formation potential (OFP) have been computed following equations (1) and (2).

As previously mentioned, the total concentrations of studied VOC are in the same order of magnitude in the three contrasting regions. However, kiVOCi and OFP values differ from one area to another. For instance, similar OFP estimated values are observed in Paris (462 OFP-

relative ppb) and WMB regions (450 OFP-relative ppb and 526 OFP-relative ppb including HCHO), while the OFP is three times higher in SWA (1228 OFP-relative ppb and 1406 including HCHO). This difference is mainly associated with the higher concentrations of acetaldehyde and isoprene observed in the SWA region. BVOC are found to be the highest contributors to OFP in Paris, WMB, and SWA, between 50% and up to 60% in Paris, usually followed by OVOC (30%-44%) and AVOC (4-28%) both inside and outside the urban plumes. The high contribution of OVOC observed in SWA is due to flight 18 during DACCIWA, which flew over forested areas, indicating that there should be primary or secondary production of OVOC from biogenic sources.

The averaged OH loss rate, calculated by the (k_iVOC_i), equals 4.03 s^{-1} in Paris, 3.2 s^{-1} in WMB and 11.4 s^{-1} in SWA. The airborne total OH loss rate is first compared to the one measured at ground level at an urban Paris site during the wintertime MEGAPOLI campaign (Dolgorouky et al., 2012) and at a remote site in Cape Corsica during the summertime SAFMED campaign (Zannoni et al., 2017); those values equal 33 s-1 (median) down to (limit of detection) in Paris and 3 (limit of detection) and 17 s^{-1} in Cape Corsica. Our values are similar to those reported in previous studies, given that the total measured OH loss rate in Paris represents an upper limit compared with summertime. One should also keep in mind that the Q-PTR-MS only measured some of the major O/VOC but not all of the wide VOC spectrum. As a consequence, we have calculated and reported in Figure 4 the average OH loss rate from ground-based VOC observations performed during the aircraft campaign by only selecting the same compounds. The calculated ground-based values of OH loss rate equal to 1.48 ± 0.89 s^{-1} in Paris in summertime (Baudic et al., 2016), 0.99 ± 0.91 s^{-1} in Cape Corsica (Ersa, Michoud et al., 2017) and 2.63 ± 1.97 s^{-1} in Abidjan, Côte d'Ivoire (Dominutti et al., 2019). The calculated OH loss rates are in the same order of magnitude, except in SWA,

where the differences between airborne and ground-based platforms can be explained by the lack of OVOCs measurements at the ground.

The contribution of the three VOC groups studied in this article to the total ·OH loss rate is in good agreement with the results obtained for the OFP. BVOCs have the largest average contribution to the ·OH loss rate, with a total contribution of 80.5 % in Paris (52.4 % on the ground), 52.1 % in WMB (76.9% on the ground), and 68.3 % in SWA (60 % on the ground). Regarding the potential interferences for isoprene (see section 2.2.1), Coggon and co-workers evaluated a 50% maximum interference in urban environments. Assuming a 50% contribution of anthropogenic interferences to isoprene (an upper limit), the BVOC still dominate the OH loss rate in the explored plumes.

OVOC dominate the ·OH loss rate after BVOC in Paris (14 %, 37% on the ground) and SWA (28.9 %, no data available on the ground). Nevertheless, in WMB, OVOC has the minimum contribution to the OH loss rate (17 % and 21% on the ground). On the other hand, AVOCs contribute only 5.8 % to the ·OH loss rate in Paris (10% on the ground) and 3 % in SWA (40% on the ground), while it is as high as 31.2 % in the WMB (2% at the ground).

The differences in the OH loss rate between airborne and ground measurements are mainly related to the chemical processing of the air masses observed, with a higher contribution of OVOCs and BVOCs (and their oxidation products) in the airborne studies and a higher contribution of primary emissions (like AVOCs) in ground-based measurements. This is different in WMB since ground-based measurements were performed at a remote site under the influence of processed air masses (Zanonni et al., 2017). Finally, the differences in the mixing ratios observed inside vs. outside the plume are not detected in the photochemistry indicators evaluated except for Paris, which presents a slightly higher OH loss rate outside than inside the plumes (Figure 4).

Given the limited number of O/VOC detected by the Q-PTR-MS, the representativeness of the observed contributions of the AVOC, BVOC and OVOC families to the OH loss rates within the plumes is now discussed. For that purpose, we rely on the paper by Zannoni et al. (2017) at the remote site of Cape Corsica, where a wider range of VOC was measured compared with the one detected by the airborne Q-PTR-MS. In Paris, Dolgorouky et al. (2012) also reported the contributions of various inorganic (NOx and CO) and VOC families to the OH loss rate from megacities worldwide, like Mexico and Tokyo. NOx usually explains around half of the OH loss rate, while BVOC are close to 1% at ground-based sites. Given the urban nature of those sites, which are freshly impacted by NOx emitters (traffic) and are surrounded by few green areas, the BVOC are not expected to make a significant contribution to the OH loss rate. Compared to the remote site of Cape Corsica, the comparison with near-source sites is not relevant here. Despite the wider range of measured VOC among AVOC, BVOC and OVOC, the contribution of BVOC at Cape Corsica is still significant, explaining at least 45% of the measured OH loss rate during the daytime. The contribution of AVOC and BVOC is lower, explaining at least 12% and 19% of the OH loss rate, respectively. Despite the limited number of the measured species, the airborne Q-PTR-MS provides a relevant fingerprint of the biogenic, anthropogenic and oxygenated contributions to the OH loss rate.

Figure 5 shows OPF and kiVOCi reactivity for each VOC species in descending order in Paris, WMB, and SWA. Similar species presented a different order of the OFP-relative ppb and kiVOCi reactivity contributions in each area. In some previous studies, aromatic compounds were the most dominant species in terms of reactivity and contribution to ozone formation in the urban area of Shanghai (Cai et al., 2010), in rural and remote areas of Guangzhou (Tang et al., 2007) and an industrial site in Southern Taiwan (Chang et al., 2005) and from an aircraft observation in Seoul (Simpson et al., 2020). However, isoprene was

found to have the most significant OFP, and aromatics compounds represent the least significant ones in the studies of Yan et al. (2017), Na et al. (2005) and Zheng et al. (2009).

In Paris, the major VOC species contributing to OFP are isoprene (39.2 %), acetaldehyde (20.9 %), MACR+MVK (14.5 %), methanol (6.9 %) and monoterpenes (4.2 %). These top five species account for 85.7 % of the total OFP contribution. Similarly, the top five VOC species contributing to the total ·OH loss rate are isoprene (65.3 %), acetaldehyde (11.3 %), MACR+MVK (7.4 %), monoterpenes (7.4 %) and C_9 aromatics (2.6 %). They account for 94 % of the total kiVOCi contribution (Figure 7).

In WMB, the top 5 VOC species for OFP are MACR+MVK (40.6 %), C_9 aromatics (22.2 %), acetaldehyde (12.8 %), methanol (7.8%) and monoterpenes (6.6 %), accounting for 90 % of the total OFP. The most photochemically relevant species towards ·OH are MACR+MVK (31.6 %), C_9 aromatics (26.9 %), monoterpenes (17 %), acetaldehyde (15.1 %) and methanol (4.2 %), attributing 94.8 % of the total ·OH loss rate.

In SWA, the most photochemically relevant species are acetaldehyde (36.2 % for OFP and 26.5 % kiVOCi), isoprene (36 % for OFP and 57.7 % for kiVOCi), HCHO (12.6 % for OFP and 6.3 % for kiVOCi), MACR+MVK (6.8 % for OFP and 3.7 % for kiVOCi) and monoterpenes (1.7 % for OFP and 2.5 % for kiVOCi). These species explain 93.3% and 96.7 % of the total OFP and kiVOCi, respectively.

3.3.2 Spatial and temporal distribution of oxidants during the flights

The time series and the spatial distribution of major trace gases provide a first insight into the oxidative processing of the plumes. An illustration is provided with the northern flight 36 during Paris-MEGAPOLI in Figures 6 and 7 and flight 19 during SWA-DACCIWA (Figures S1 and S2 in the Supplement Material). Figures 6 and S2 report the 2D flight trajectory color-coded by the NOx, Ox and selected VOC mixing ratios. Figure 7 shows the time series of

NOx or CO along with AVOC species (toluene, C_8 and C_9 aromatics), BVOC and OVOC (acetone and acetaldehyde).

Despite their significant regional background levels, the 2D trajectories (Figure 6) reveal the well-defined edges of the Paris plume for anthropogenic compounds and even OVOC (Figure 6). The distribution of BVOC shows a different feature: while the distribution of isoprene (m/z 69) seems independent of the Paris plume's position, this of its oxidation products (MACR+MVK, m/z 71) is impacted. One should note that isoprene and its oxidation products show their highest levels in the sector of the Rambouillet forest in southwestern Paris. Interestingly, the location of the Ox plume is slightly shifted to the west at the edges of the plume (Figure 6). Due to different flight trajectory, the spatial feature of the DACCIWA flight 19 is less explicit. As expected, NOx and AVOC show their highest levels downwind the ACCRA's plume. BVOC show their highest levels when the aircraft flies over the forested areas in the western part of Lome. OVOC show their highest levels downwind of the ACCRA's plume and in the Northern part of the DACCIWA domain.

As noted in Figure 7, NOx peaks mark the crossing of the Paris plume by the ATR-42 aircraft, as already discussed in Thera et al. (2022). A simultaneous increase in AVOC and OVOC mixing ratios, well above their background levels, is observed for each plume transect (and CO – not shown here). However, the mixing ratios of these compounds decrease with time as long as the aircraft travels away from the Paris centre. Indeed, C_9-aromatics decrease more rapidly than benzene and toluene due to their higher coefficient rates towards the ·OH radical (1.45×10^{-11} versus 1.20×10^{-12} cm^{-3} $molecules^{-1}$ s^{-1}) by being consumed faster in the plume. For the DACCIWA flight 19, there is no clear indication of oxidative processing with time; this is probably due to the exploration of different urban plumes, which differ from the pseudo-lagrangian exploration of one single plume in Paris during MEGAPOLI.

The spatial distribution and time series provide a first qualitative insights into the chemical processing occurring inside the urban plumes. The decay rate of O/VOC and the secondary production of OVOC and Ox are going to be quantified in the following section in order to evaluate the magnitude of the chemical processing.

3.3.3 Cumulative oxidant production vs. ·OH exposure

To compute oxidant production vs. ·OH exposure, a decrease in NO_x and CO levels has to be observed inside the plume. While this decrease was observed in three of the four selected flights of MEGAPOLI, none was observed inside SWA plumes. Consequently, oxidants' production could only be computed for MEGAPOLI-selected flights. Figure 8 depicts the correlation between Δ[Ox]/Δ[CO], which is plotted against the cumulative ·OH exposure (Δt[OH]) for flights 32, 33, and 36 of the MEGAPOLI campaign. The scatterplots represent the average oxidant production of each plume intercepted during each flight. As expected, Δ[Ox]/Δ[CO] increases with Δt[OH], and they all present significant determination coefficients (R^2 ranges between 0.58 and 0.93). Wood et al. (2009) also obtained an increase in oxidant production with ·OH exposure with a correlation > 0.90 in Mexico City from an Aerodyne mobile laboratory. The slopes of the linear fit are 3.3×10^{-11} and 3.1×10^{-11} ppb_v Ox /ppb_v CO (molecules s $cm^{-3})^{-1}$ for flights 32 and 36, respectively, at ±55%. That value gets higher for flight 33 : it equal 3.4×10^{-10} ppb_v Ox /ppb_v CO (molecules s $cm^{-3})^{-1}$. Surprisingly these values are 10 to 100 times higher than those reported in Wood et al. (2009) (for flights 32-36 and 33, respectively), whose slopes ranged between 3.6 and 5.6×10^{-12} ppb_v Ox/ppb_v CO (molecules s $cm^{-3})^{-1}$ in Mexico City. Note that the slope from Mexico City was derived from the full-day values, which are expected to be higher during the afternoon. The reasons for such discrepancies could be the differences in VOC reactivity loadings, the NOx levels, and more favorable photochemical conditions.

3.3.4 The decay and production of O/VOC

Figure 9 displays the scatterplot of the ΔVOC-to-ΔCO against the processing time inside the plumes and the mean and standard deviations of ΔVOC-to-ΔCO calculated for each plume transect. A decay of the averaged ΔVOC-to-ΔCO (illustrated by C_8-aromatics) is observed for flights 25, 27, 33 and 36 of MEGAPOLI, fitting a linear least-square regression slope with an R^2 higher than 0.80 except for flight 33 (0.54). Primary decays observed for C_8-aromatics range from 0.87 to 3.19 ppt_v VOC ppb_v^{-1} CO per hour on average. The highest decay is observed during flight 36, with a total of 3.19 ppt_v ppb_v^{-1} CO per hour, depicting a faster reaction and consumption of the C_8-aromatics. Linear fits are reported in Table 3 for all AVOC during the four MEGAPOLI flights. Aromatic AVOC usually show a linear decay with the processing time of the plume, but the significance of the fit is not always met. During flight #36, the R^2 of the benzene and toluene's fit is weak (< 0.30), and the standard error of the slope is high (115% of the slope for toluene), moderating the observed averaged decay rate. The examination of the time series for flight 36 (not shown here) already suggested that toluene mixing ratios stayed proportional to the ones of benzene during the plume intercept. The same behaviour was previously observed in the Los Angeles plume, where, despite a 3 to 5 hour-transport time, the proportion between toluene and benzene did not change between the source and the receptor (Borbon et al., 2013). It suggests that the reactivity towards the OH of benzene and toluene is not high enough to be captured during this transport time. The differences observed between the plumes could be related to the concentrations of oxidants inside the plumes and the atmospheric conditions favouring the decay of these compounds. The C_8-aromatics usually show the greatest decay rate inside the urban plume compared to benzene and toluene, which is explained by their higher rate constants with OH (by an order of magnitude).

Figure 10 displays the scatter plot of the ΔOVOC/ΔCO ratios versus the processing time of the plume for flights 33 and 36 of MEGAPOLI. Depending on the flight, either a production or a decay is depicted for the different OVOC species. During flight 33, OVOC enhancement ratios show a strong production fitting a linear least square regression slope ($r^2 \geq 0.85$, except for MACR + MVK and methanol, Table 3). There is 17.9±2 ppt_v of acetaldehyde produced per ppb_v of CO per hour in the plume, presenting the highest OVOC production inside the plume. The production rate ranges between 4.37 and 18 ppt_v VOC ppb_v^{-1} CO per hour on average. Production is also depicted during flight #27 but at a lower production rate (by one order of magnitude lower) and with a lower R^2 (around 0.50), and the absence of production of methanol during this flight is observed ($R^2 = 0.01$). The OVOC production during flight 33 is the strongest of the whole campaign.

The primary biogenic nature of OVOC and its potential bias to the observed OVOC production are discussed here by taking the MEGAPOLI flight 33 as an example. Figure S3 shows the time series of trace gases of interest as well as the colour-coded plot trajectories for flight 33 of MEGAPOLI. This flight was performed in the eastern sector of Paris, downwind of the Paris plume. Contrary to AVOC, figure S3 displays that the mixing ratios of OVOC (illustrated by acetone and methanol) increase as long as the ATR-42 moves away from the urban area (Paris, France) but independently of the urban plume intercept. Moreover, isoprene, a biogenic marker, shows higher mixing ratios outside the urban plume. The increase of OVOC and isoprene mixing ratios indicate the potential biogenic contribution of the regional background as long as the aircraft flies over the rural and forested areas surrounding Paris. The potential contribution of a biogenic regional background is subtracted through the Δ[OVOC] term, as described in Equation 3. Consequently, the primary biogenic contribution of OVOC does not bias the calculation of their production rates inside the plume. The intensity of the production rates of OVOC inside the urban plumes is also modulated by

their sink terms (mainly oxidation by the OH radical and, for some of them, by photolysis like acetone).

Apart from flights 27 and 33 and methanol and acetone during flight 25, OVOC either show a clear decay as a function of the plume processing time (MACR+MVK and MEK during flight 25) or no clear production associated with low R^2 (flight 36) as well as any plume in SWA (Table 3). However, the decay rates of OVOCs are lower than the production ones observed during flight 33. In addition, except for flight 33 where acetaldehyde depicted a clear production, no clear production or decay is observed for this compound in other flights.

4. Conclusions

This study aimed to evaluate the composition, primary and secondary sources, and the reactivity (production and decay rates) of the O/VOC burden in polluted plumes in three contrasting regions: Paris, North West Mediterranean Basin (WMB) and South West Africa (SWA). The polluted plumes were explored by the French research aircraft ATR-42 during the intensive campaigns of the international MEGAPOLI, SAFMED/ChArMEx and DACCIWA projects. For our purpose, various reactivity metrics have been applied to the trace gases collected onboard the ATR-42. O/VOC species were measured by a Q-PTR-MS, which showed a robust and consistent response over the last decade.

Our study is constrained primarily by the restricted number of measured VOC species across various study areas. This limitation may result in potential overestimation or underestimation when compared to prior studies. Nonetheless, the robust aspect of our research lies in the incorporation of a unique and distinctive dataset, offering valuable insights into VOC levels and reactivity in regions that are both contrasting and less explored.

Oxygenated VOCs dominate the air mass composition in the three contrasting regions, explaining 70 % of the total VOC mixing ratios. Even if a small number of OVOCs were

measured in the different areas of our studies, a higher contribution of these species was also observed in previous studies in urban areas, suggesting the contribution from primary and secondary sources. While the total VOC burden is higher in SWA plumes compared to Paris and the WMB ones, the distribution between BVOC, AVOC, and OVOC is still consistent.

Regarding the reactivity of the plume, biogenic VOCs (BVOC) are the greatest contributors both inside and outside the polluted plumes in the three regions. While an anthropogenic origin of some BVOC, such as terpenoids (isoprene and monoterpenes), is not excluded, our results strengthen the importance of taking into account the biogenic fraction of gaseous precursors in urban areas to address atmospheric chemistry issues.

The total OH loss rate obtained was 4.03 and 3.2 s^{-1} in Paris and WMB, respectively, while it is 3 times higher in SWA (12.1 s^{-1}) on average. Moreover, the ozone formation potential varies between 400 and 1200 OFP-relative ppb in the three contrasting areas. These values are within the same range or in the lower limit of the ones measured at ground-based sites in Ersa (Mediterranean) and Paris, respectively. Despite the limited number of the measured species, the airborne Q-PTR-MS provides a relevant fingerprint of the biogenic, anthropogenic and oxygenated contributions to the OH loss rate through the comparison with the ground-based larger dataset. They also confirm the recent studies in contrasted environment from northern latitudes (see for instance Pfannerstill et al.,(2023) in Los Angeles to lower latitudes like Borbon et al. (2024) in Beiru,Lebanon) and Sarkar et al. (2017) in the Katmandu Valley, Nepal.

The chemical processing is examined and quantified in the Paris plumes by linking the. $\Delta[X]/\Delta[CO]$ and the processing of the plume through $\Delta t[OH]$ exposure and the time processing. AVOC (aromatics) show a decay rate between -0.5 and -3.2 ppt_{AVOC} ppb_{CO}^{-1} per hour, while OVOC either show an increase (secondary production) or a decrease. The

production rate is by far the strongest, up to 18 ppt_{OVOC} ppb_{CO}^{-1} per hour (acetaldehyde) during the eastern flight 33 in Paris.

This study presents an unprecedented ensemble of airborne campaigns over contrasting areas of the developed and developing world to assess the chemical and spatial O/VOC distributions, their reactivity and implications in atmospheric chemistry, emphasizing the importance of oxygenated and biogenic VOC in urban plumes. For future studies, the implementation of a photochemistry model along the flight paths could bring new insights into the data and the chemical processing of the plumes. This could also provide a better understanding of VOC reactivity and the main processes impacting their lifetime in these contrasting regions.

Acknowledgements

Airborne data were obtained using the ATR-42 aircraft managed by SAFIRE, the French facility for airborne research, an infrastructure of the French National Center for Scientific Research (CNRS), Meteo-France and the French National Center for Space Studies (CNES). Part of the research leading to these results has received funding from the European Union's Seventh Framework Programme FP/2007-2011 within the project MEGAPOLI, grant agreement 212520. The authors also acknowledge their financial support to both the ANR through the MEGAPOLI PARIS project and the INSU/LEFE program through the MEGAPOLI France project. This study also received financial support from MISTRALS by ADEME, CEA, INSU, and Meteo-France and from ANR through the SAFMED project (grant number ANR-12-BS060013-2502). Finally, this work has received funding from the European Union Seventh Framework Programme (FP7/20072013) under grant agreement number 603502 (EU project DACCIWA: dynamics-aerosol-chemistry-cloud interactions in

West Africa). The authors are grateful to the people who contributed to implementing the formaldehyde analyzer and the Q-PTR-MS on the field: Joel Brito, Laëtitia Bouvier, Servanne Chevaillier, Cécile Gaimoz, Noël Grand and Sylvain Triquet. The authors also address a special thanks to the pilots and flight crew from Safire for their enthusiasm and support during the measurement campaigns aboard the ATR 42 aircraft.

5. References

Ait-Helal, W., Borbon, A., Sauvage, S., Gouw, J.A. de, Colomb, A., Gros, V., Freutel, F., Crippa, M., Afif, C., Baltensperger, U., Beekmann, M., Doussin, J.-F., Durand-Jolibois, R., Fronval, I., Grand, N., Leonardis, T., Lopez, M., Michoud, V., Miet, K., Perrier, S., Prévôt, A.S.H., Schneider, J., Siour, G., Zapf, P., Locoge, N., 2014. Volatile and intermediate volatility organic compounds in suburban Paris: variability, origin and importance for SOA formation. Atmospheric Chem. Phys. 14, 10439–10464. https://doi.org/10.5194/acp-14-10439-2014

Apel, E.C., Emmons, L.K., Karl, T., Flocke, F., Hills, A.J., Madronich, S., Lee-Taylor, J., Fried, A., Weibring, P., Walega, J., Richter, D., Tie, X., Mauldin, L., Campos, T., Weinheimer, A., Knapp, D., Sive, B., Kleinman, L., Springston, S., Zaveri, R., Ortega, J., Voss, P., Blake, D., Baker, A., Warneke, C., Welsh-Bon, D., Gouw, J. de, Zheng, J., Zhang, R., Rudolph, J., Junkermann, W., Riemer, D.D., 2010. Chemical evolution of volatile organic compounds in the outflow of the Mexico City Metropolitan area. Atmospheric Chem. Phys. 10, 2353–2375. https://doi.org/10.5194/acp-10-2353-2010

Baudic, A., Gros, V., Sauvage, S., Locoge, N., Sanchez, O., Sarda-Estève, R., Kalogridis, C., Petit, J.E., Bonnaire, N., Baisnée, D., Favez, O., Albinet, A., Sciare, J., Bonsang, B., 2016. Seasonal variability and source apportionment of volatile organic compounds (VOCs) in the Paris megacity (France). Atmospheric Chem. Phys. 16, 11961–11989. https://doi.org/10.5194/acp-16-11961-2016

Borbon, A., Gilman, J.B., Kuster, W.C., Grand, N., Chevaillier, S., Colomb, A., Dolgorouky, C., Gros, V., Lopez, M., Sarda-Esteve, R., Holloway, J., Stutz, J., Petetin, H., McKeen, S., Beekmann, M., Warneke, C., Parrish, D.D., Gouw, J.A. de, 2013. Emission ratios of anthropogenic volatile organic compounds in northern mid-latitude megacities: Observations versus emission inventories in Los Angeles and Paris. J. Geophys. Res. Atmospheres 118, 2041–2057. https://doi.org/10.1002/jgrd.50059

Borbon, A., Ruiz, M., Bechara, J., Aumont, B., Chong, M., Huntrieser, H., Mari, C., Reeves, C.E., Scialom, G., Hamburger, T., Stark, H., Afif, C., Jambert, C., Mills, G., Schlager, H., Perros, P.E., 2012. Transport and chemistry of formaldehyde by mesoscale convective systems in West Africa during AMMA 2006. J. Geophys. Res. Atmospheres 117, n/a-n/a. https://doi.org/10.1029/2011JD017121

Borbon, A., Afif, C., Salameh, T., Sauvage, S., Light oxygenated volatile organic compound concentrations in an Eastern Mediterranean urban atmosphere rivalling those in megacities, Env. Poll.,. In press, 2024.

Brito, J., Freney, E., Dominutti, P., Borbon, A., Haslett, S.L., Batenburg, A.M., Colomb, A., Dupuy, R., Denjean, C., Burnet, F., Bourriane, T., Deroubaix, A., Sellegri, K., Borrmann, S., Coe, H., Flamant, C., Knippertz, P., Schwarzenboeck, A., 2018. Assessing the role of anthropogenic and biogenic sources on PM₁ over southern West Africa using aircraft measurements. Atmospheric Chem. Phys. 18, 757–772. https://doi.org/10.5194/acp-18-757-2018

Cai, C., Geng, F., Tie, X., Yu, Q., An, J., 2010. Characteristics and source apportionment of VOCs measured in Shanghai, China. Atmos. Environ. 44, 5005–5014.

Coggon, M.M., Stockwell, C.E., Claflin, M.S., Pfannerstill, E.Y., Lu, X., Gilman, J.B., Marcantonio, J., Cao, C., Bates, K., Gkatzelis, G.I., Lamplugh, A., Katz, E.F., Arata, C., Apel, E.C., Hornbrook, R.S., Piel, F., Majluf, F., Blake, D.R., Wisthaler, A., Canagaratna, M., Lerner, B.M., Goldstein, A.H., Mak, J.E., Warneke, C., 2023. Identifying and correcting interferences to PTR-ToF-MS measurements of isoprene and other urban volatile organic compounds (preprint). Gases/In Situ Measurement/Instruments and Platforms. https://doi.org/10.5194/egusphere-2023-1497

Colomb, A., Williams, J., Crowley, J., Gros, V., Hofmann, R., Salisbury, G., Klüpfel, T., Kormann, R., Stickler, A., Forster, C., Lelieveld, J., 2006. Airborne Measurements of

Trace Organic Species in the Upper Troposphere Over Europe: the Impact of Deep Convection. Environ. Chem. 3, 244–259.

Crawford, J.H., Ahn, J.-Y., Al-Saadi, J., Chang, L., Emmons, L.K., Kim, J., Lee, G., Park, J.-H., Park, R.J., Woo, J.H., Song, C.-K., Hong, J.-H., Hong, Y.-D., Lefer, B.L., Lee, M., Lee, T., Kim, S., Min, K.-E., Yum, S.S., Shin, H.J., Kim, Y.-W., Choi, J.-S., Park, J.-S., Szykman, J.J., Long, R.W., Jordan, C.E., Simpson, I.J., Fried, A., Dibb, J.E., Cho, S., Kim, Y.P., 2021. The Korea–United States Air Quality (KORUS-AQ) field study. Elem. Sci. Anthr. 9, 00163. https://doi.org/10.1525/elementa.2020.00163

Debevec, C., Sauvage, S., Gros, V., Salameh, T., Sciare, J., Dulac, F., Locoge, N., 2021. Seasonal variation and origins of volatile organic compounds observed during 2 years at a western Mediterranean remote background site (Ersa, Cape Corsica). Atmospheric Chem. Phys. 21, 1449–1484. https://doi.org/10.5194/acp-21-1449-2021

Delmas, R., Megie, G., Peuch, V.H., 2005. Atmosphere physics and chemistry; Physique et chimie de l'atmosphere, []. Editions Belin, Paris (France), France.

Denjean, C., Bourrianne, T., Burnet, F., Mallet, M., Maury, N., Colomb, A., Dominutti, P., Brito, J., Dupuy, R., Sellegri, K., Schwarzenboeck, A., Flamant, C., Knippertz, P., 2020. Overview of aerosol optical properties over southern West Africa from DACCIWA aircraft measurements. Atmospheric Chem. Phys. 20, 4735–4756. https://doi.org/10.5194/acp-20-4735-2020

Derwent, R.G., Jenkin, M.E., Pilling, M.J., Carter, W.P.L., Kaduwela, A., 2010. Reactivity scales as comparative tools for chemical mechanisms. J. Air Waste Manag. Assoc. 1995 60, 914–924. https://doi.org/10.3155/1047-3289.60.8.914

Dolgorouky, C., Gros, V., Sarda-Esteve, R., Sinha, V., Williams, J., Marchand, N., Sauvage, S., Poulain, L., Sciare, J., Bonsang, B., 2012. Total OH reactivity measurements in Paris during the 2010 MEGAPOLI winter campaign. Atmospheric Chem. Phys. 12, 9593–9612. https://doi.org/10.5194/acp-12-9593-2012

Dominutti, P., Keita, S., Bahino, J., Colomb, A., Liousse, C., Yoboué, V., Galy-Lacaux, C., Morris, E., Bouvier, L., Sauvage, S., Borbon, A., 2019. Anthropogenic VOCs in Abidjan, southern West Africa: from source quantification to atmospheric impacts. Atmospheric Chem. Phys. 19, 11721–11741. https://doi.org/10.5194/acp-19-11721-2019

Duren, R.M., Miller, C.E., 2012. Measuring the carbon emissions of megacities. Nat. Clim. Change 2, 560–562. https://doi.org/10.1038/nclimate1629

Dusanter, S., Vimal, D., Stevens, P.S., Volkamer, R., Molina, L.T., 2009. Measurements of OH and HO2 concentrations during the MCMA-2006 field campaign – Part 1: Deployment of the Indiana University laser-induced fluorescence instrument. Atmos Chem Phys.

Filges, A., Gerbig, C., Chen, H., Franke, H., Klaus, C., Jordan, A., 2015. The IAGOS-core greenhouse gas package: a measurement system for continuous airborne observations of CO 2 , CH 4 , H 2 O and CO. Tellus B Chem. Phys. Meteorol. 67, 27989. https://doi.org/10.3402/tellusb.v67.27989

Finlayson-Pitts, B., Pitts, J.N., 2000. Chemistry of the Upper and Lower Atmopshere, 1st editio. ed. Academic Press.

Flamant, C., Knippertz, P., Fink, A.H., Akpo, A., Brooks, B., Chiu, C.J., Coe, H., Danuor, S., Evans, M., Jegede, O., Kalthoff, N., Konaré, A., Liousse, C., Lohou, F., Mari, C., Schlager, H., Schwarzenboeck, A., Adler, B., Amekudzi, L., Aryee, J., Ayoola, M., Batenburg, A.M., Bessardon, G., Borrmann, S., Brito, J., Bower, K., Burnet, F., Catoire, V., Colomb, A., Denjean, C., Fosu-Amankwah, K., Hill, P.G., Lee, J., Lothon, M., Maranan, M., Marsham, J., Meynadier, R., Ngamini, J.-B., Rosenberg, P., Sauer, D., Smith, V., Stratmann, G., Taylor, J.W., Voigt, C., Yoboué, V., 2018. The Dynamics–Aerosol–Chemistry–Cloud Interactions in West Africa Field Campaign: Overview and Research Highlights. Bull. Am. Meteorol. Soc. 99, 83–104. https://doi.org/10.1175/BAMS-D-16-0256.1

Freney, E., Sellegri, K., Chrit, M., Adachi, K., Brito, J., Waked, A., Borbon, A., Colomb, A., Dupuy, R., Pichon, J.M., Bouvier, L., Delon, C., Jambert, C., Durand, P., Bourianne, T., Gaimoz, C., Triquet, S., Féron, A., Beekmann, M., Dulac, F., Sartelet, K., 2018. Aerosol composition and the contribution of SOA formation over Mediterranean forests. Atmospheric Chem. Phys. 18, 7041–7056. https://doi.org/10.5194/acp-18-7041-2018

Freney, E.J., Sellegri, K., Canonaco, F., Colomb, A., Borbon, A., Michoud, V., Crumeyrolle, S., Amarouche, N., Bourianne, T., Gomes, L., Prevot, A.S.H., Beekmann, M., Schwarzenböeck, A., 2014. Characterizing the impact of urban emissions on regional aerosol particles: Airborne measurements during the MEGAPOLI experiment. Atmospheric Chem. Phys. 14, 1397–1412. https://doi.org/10.5194/acp-14-1397-2014

Guenther, A., 2000. Natural emissions of non-methane volatile organic compounds, carbon monoxide, and oxides of nitrogen from North America. Atmos. Environ. 34, 2205–2230. https://doi.org/10.1016/S1352-2310(99)00465-3

Hak, C., Pundt, I., Kern, C., Platt, U., Dommen, J., Ordóñez, C., Prévôt, a S.H., Junkermann, W., Astorga-Lloréns, C., Larsen, B.R., Mellqvist, J., Strandberg, a, Yu, Y., Galle, B., Kleffmann, J., Lörzer, J.C., Braathen, G.O., Volkamer, R., 2005. Intercomparison of four different in-situ techniques for ambient formaldehyde measurements in urban air. Atmospheric Chem. Phys. Discuss. 5, 2897–2945. https://doi.org/10.5194/acpd-5-2897-2005

Herndon, S.C., Onasch, T.B., Wood, E.C., Kroll, J.H., Canagaratna, M.R., Jayne, J.T., Zavala, M.A., Knighton, W.B., Mazzoleni, C., Dubey, M.K., Ulbrich, I.M., Jimenez, J.L., Seila, R., Gouw, J.A. de, Foy, B. de, Fast, J., Molina, L.T., Kolb, C.E., Worsnop, D.R., 2008. Correlation of secondary organic aerosol with odd oxygen in Mexico City. Geophys. Res. Lett. 35, L15804. https://doi.org/10.1029/2008GL034058

Hoerger, C.C., Claude, A., Plass-Duelmer, C., Reimann, S., Eckart, E., Steinbrecher, R., Aalto, J., Arduini, J., Bonnaire, N., Cape, J.N., Colomb, A., Connolly, R., Diskova, J., Dumitrean,

P., Ehlers, C., Gros, V., Hakola, H., Hill, M., Hopkins, J.R., Ja¨ger, J., Junek, R., Kajos, M.K., Klemp, D., Leuchner, M., Lewis, A.C., Locoge, N., Maione, M., Martin, D., Michl, K., Nemitz, E., O'Doherty, S., Ballesta, P.P., Ruuskanen, T.M., Sauvage, S., Schmidbauer, N., Spain, T.G., Straube, E., Vana, M., Vollmer, M.K., Wegener, R., Wenger, A., 2015. ACTRIS non-methane hydrocarbon intercomparison experiment in Europe to support WMO GAW and EMEP observation networks. Atmospheric Meas. Tech. 8, 2715–2736. https://doi.org/10.5194/amt-8-2715-2015

Hoornweg, D., Pope, K., 2017. Population predictions for the world's largest cities in the 21st century. Environ. Urban. 29, 195–216. https://doi.org/10.1177/0956247816663557

Hopkins, J.R., Evans, M.J., Lee, J.D., Lewis, A.C., Marsham, J.H., McQuaid, J.B., Parker, D.J., Stewart, D.J., Reeves, C.E., Purvis, R.M., 2009. Direct estimates of emissions from the megacity of Lagos. Atmospheric Chem. PhysicsAtmospheric Chem. Phys. 9, 8471–8477. https://doi.org/10.5194/acpd-9-8667-2009

Hornbrook, R.S., Blake, D.R., Diskin, G.S., Fried, A., Fuelberg, H.E., Meinardi, S., Mikoviny, T., Richter, D., Sachse, G.W., Vay, S.A., Walega, J., Weibring, P., Weinheimer, A.J., Wiedinmyer, C., Wisthaler, A., Hills, A., Riemer, D.D., Apel, E.C., 2011. Observations of nonmethane organic compounds during ARCTAS − Part 1: Biomass burning emissions and plume enhancements. Atmospheric Chem. Phys. 11, 11103–11130. https://doi.org/10.5194/acp-11-11103-2011

Hui, L., Liu, X., Tan, Q., Feng, M., An, J., Qu, Y., Zhang, Y., Jiang, M., 2018. Characteristics, source apportionment and contribution of VOCs to ozone formation in Wuhan, Central China. Atmos. Environ. 192, 55–71. https://doi.org/10.1016/j.atmosenv.2018.08.042

Jenkin, M.E., Derwent, R.G., Wallington, T.J., 2017. Photochemical ozone creation potentials for volatile organic compounds: Rationalization and estimation. Atmos. Environ. 163, 128–137. https://doi.org/10.1016/j.atmosenv.2017.05.024

Kansal, A., 2009. Sources and reactivity of NMHCs and VOCs in the atmosphere: A review. J. Hazard. Mater. 166, 17–26. https://doi.org/10.1016/j.jhazmat.2008.11.048

Karl, T., Striednig, M., Graus, M., Hammerle, A., Wohlfahrt, G., 2018. Urban flux measurements reveal a large pool of oxygenated volatile organic compound emissions. Proc. Natl. Acad. Sci. 115, 201714715. https://doi.org/10.1073/pnas.1714715115

Kleinman, L.I., Springston, S.R., Daum, P.H., Lee, Y.-N., Nunnermacker, L.J., Senum, G.I., Wang, J., Weinstein-Lloyd, J., Alexander, M.L., Hubbe, J., Ortega, J., Canagaratna, M.R., Jayne, J., 2008. The time evolution of aerosol composition over the Mexico City plateau. Atmospheric Chem. Phys. 8, 1559–1575. https://doi.org/10.5194/acp-8-1559-2008

La Colla, N.S., Botté, S.E., Marcovecchio, J.E., 2021. Atmospheric particulate pollution in South American megacities. Environ. Rev. 29, 415–429. https://doi.org/10.1139/er-2020-0105

Langford, B., Misztal, P.K., Nemitz, E., Davison, B., Helfter, C., Pugh, T.A.M., MacKenzie, A.R., Lim, S.F., Hewitt, C.N., 2010. Fluxes and concentrations of volatile organic compounds from a South-East Asian tropical rainforest. Atmospheric Chem. Phys. 10, 8391–8412. https://doi.org/10.5194/acp-10-8391-2010

Lelieveld, J., Hadjinicolaou, P., Kostopoulou, E., Chenoweth, J., Maayar, M.E., Giannakopoulos, C., Hannides, C., Lange, M.A., Tanarhte, M., Tyrlis, E., Xoplaki, E., 2012. Climate change and impacts in the Eastern Mediterranean and the Middle East. Clim. Change 114, 667–687. https://doi.org/10.1007/s10584-012-0418-4

Liu, F., Beirle, S., Zhang, Q., Dörner, S., He, K., Wagner, T., 2016. NOx lifetimes and emissions of cities and power plants in polluted background estimated by satellite observations. Atmospheric Chem. Phys. 16, 5283–5298. https://doi.org/10.5194/acp-16-5283-2016

Ma, Z., Liu, C., Zhang, C., Liu, P., Ye, C., Xue, C., Zhao, D., Sun, J., Du, Y., Chai, F., Mu, Y., 2019. The levels, sources and reactivity of volatile organic compounds in a typical urban area of Northeast China. J. Environ. Sci. 79, 121–134. https://doi.org/10.1016/j.jes.2018.11.015

McCabe, D.C., Gierczak, T., Talukdar, R.K., Ravishankara, A.R., 2001. Kinetics of the reaction OH + CO under atmospheric conditions. Geophys. Res. Lett. 28, 3135–3138. https://doi.org/10.1029/2000GL012719

McDonald, B.C., Gouw, J.A. de, Gilman, J.B., Jathar, S.H., Akherati, A., Cappa, C.D., Jimenez, J.L., Lee-Taylor, J., Hayes, P.L., McKeen, S.A., Cui, Y.Y., Kim, S.-W., Gentner, D.R., Isaacman-VanWertz, G., Goldstein, A.H., Harley, R.A., Frost, G.J., Roberts, J.M., Ryerson, T.B., Trainer, M., 2018. Volatile chemical products emerging as largest petrochemical source of urban organic emissions. Science 359, 760–764. https://doi.org/10.1126/science.aaq0524

Michoud, V., Sciare, J., Sauvage, S., Dusanter, S., Léonardis, T., Gros, V., Kalogridis, C., Zannoni, N., Féron, A., Petit, J.-E., Crenn, V., Baisnée, D., Sarda-Estève, R., Bonnaire, N., Marchand, N., DeWitt, H.L., Pey, J., Colomb, A., Gheusi, F., Szidat, S., Stavroulas, I., Borbon, A., Locoge, N., 2017. Organic carbon at a remote site of the western Mediterranean Basin: sources and chemistry during the ChArMEx SOP2 field experiment. Atmospheric Chem. Phys. 17, 8837–8865. https://doi.org/10.5194/acp-17-8837-2017

Molina, L.T., 2021. Introductory lecture: air quality in megacities. Faraday Discuss. 226, 9–52. https://doi.org/10.1039/D0FD00123F

Monks, P.S., Granier, C., Fuzzi, S., Stohl, A., Williams, M.L., Akimoto, H., Amann, M., Baklanov, A., Baltensperger, U., Bey, I., Blake, N., Blake, R.S., Carslaw, K., Cooper, O.R., Dentener, F., Fowler, D., Fragkou, E., Frost, G.J., Generoso, S., Ginoux, P., Grewe, V., Guenther, A., Hansson, H.C., Henne, S., Hjorth, J., Hofzumahaus, A., Huntrieser, H., Isaksen, I.S.A., Jenkin, M.E., Kaiser, J., Kanakidou, M., Klimont, Z., Kulmala, M., Laj, P., Lawrence, M.G., Lee, J.D., Liousse, C., Maione, M., McFiggans, G., Metzger, A., Mieville, A., Moussiopoulos, N., Orlando, J.J., O'Dowd, C.D., Palmer, P.I., Parrish, D.D., Petzold, A., Platt, U., Pöschl, U., Prévôt, A.S.H., Reeves, C.E., Reimann, S., Rudich, Y., Sellegri,

K., Steinbrecher, R., Simpson, D., ten Brink, H., Theloke, J., van der Werf, G.R., Vautard, R., Vestreng, V., Vlachokostas, C., von Glasow, R., 2009. Atmospheric composition change - global and regional air quality. Atmos. Environ. 43, 5268–5350. https://doi.org/10.1016/j.atmosenv.2009.08.021

Murphy, J.G., Oram, D.E., Reeves, C.E., 2010. Measurements of volatile organic compounds over West Africa. Atmospheric Chem. Phys. 10, 5281–5294. https://doi.org/10.5194/acp-10-5281-2010

Nash, T., 1953. The colorimetric estimation of formaldehyde by means of the Hantzsch reaction. Biochem. J. 55, 416–421. https://doi.org/10.1042/bj0550416

Nedelec, P., Cammas, J.-P., Thouret, V., Athier, G., Cousin, J.-M., Legrand, C., Abonnel, C., Lecoeur, F., Cayez, G., Marizy, C., 2003. An improved infrared carbon monoxide analyser for routine measurements aboard commercial Airbus aircraft: technical validation and first scientific results of the MOZAIC III programme. Atmospheric Chem. Phys. 3, 1551–1564. https://doi.org/10.5194/acp-3-1551-2003

Niu, H., Mo, Z., Shao, M., Lu, S., Xie, S., 2016. Screening the emission sources of volatile organic compounds (VOCs) in China by multi-effects evaluation. Front. Environ. Sci. Eng. 10, 1. https://doi.org/10.1007/s11783-016-0828-z

Pfister, G.G., Reddy, P.J., Barth, M.C., Flocke, F.F., Fried, A., Herndon, S.C., Sive, B.C., Sullivan, J.T., Thompson, A.M., Yacovitch, T.I., Weinheimer, A.J., Wisthaler, A., 2017. Using Observations and Source-Specific Model Tracers to Characterize Pollutant Transport During FRAPPÉ and DISCOVER-AQ. J. Geophys. Res. Atmospheres 122. https://doi.org/10.1002/2017JD027257

Rantala, P., Järvi, L., Taipale, R., Laurila, T.K., Patokoski, J., Kajos, M.K., Kurppa, M., Haapanala, S., Siivola, E., Petäjä, T., Ruuskanen, T.M., Rinne, J., 2016. Anthropogenic and biogenic influence on VOC fluxes at an urban background site in Helsinki, Finland. Atmospheric Chem. Phys. 16, 7981–8007. https://doi.org/10.5194/acp-16-7981-2016

Roberts, J.M., Fehsenfeld, F.C., Liu, S.C., Bollinger, M.J., Hahn, C., Albritton, D.L., Sievers, R.E., 1984. Measurements of aromatic hydrocarbon ratios and NOx concentrations in the rural troposphere: Observation of air mass photochemical aging and NOx removal. Atmospheric Environ. 1967 18, 2421–2432. https://doi.org/10.1016/0004-6981(84)90012-X

Roukos, J., Riffault, V., Locoge, N., Plaisance, H., 2009. VOC in an urban and industrial harbor on the French North Sea coast during two contrasted meteorological situations. Environ. Pollut. 157, 3001–3009. https://doi.org/10.1016/j.envpol.2009.05.059

Ryerson, T.B., Andrews, A.E., Angevine, W.M., Bates, T.S., Brock, C.A., Cairns, B., Cohen, R.C., Cooper, O.R., de Gouw, J.A., Fehsenfeld, F.C., Ferrare, R.A., Fischer, M.L., Flagan, R.C., Goldstein, A.H., Hair, J.W., Hardesty, R.M., Hostetler, C.A., Jimenez, J.L., Langford, A.O., McCauley, E., McKeen, S.A., Molina, L.T., Nenes, A., Oltmans, S.J., Parrish, D.D., Pederson, J.R., Pierce, R.B., Prather, K., Quinn, P.K., Seinfeld, J.H., Senff, C.J., Sorooshian, A., Stutz, J., Surratt, J.D., Trainer, M., Volkamer, R., Williams, E.J., Wofsy, S.C., 2013. The 2010 California Research at the Nexus of Air Quality and Climate Change (CalNex) field study: CalNex 2010 FIELD PROJECT OVERVIEW. J. Geophys. Res. Atmospheres 118, 5830–5866. https://doi.org/10.1002/jgrd.50331

Seinfeld, J.H., Pandis, S.N., 2006. Atmospheric Chemistry and Physics. From Air Pollution to Climate Change. John Wiley & Sons.

Simpson, I.J., Blake, D.R., Blake, N.J., Meinardi, S., Barletta, B., Hughes, S.C., Fleming, L.T., Crawford, J.H., Diskin, G.S., Emmons, L.K., Fried, A., Guo, H., Peterson, D.A., Wisthaler, A., Woo, J.-H., Barré, J., Gaubert, B., Kim, J., Kim, M.J., Kim, Y., Knote, C., Mikoviny, T., Pusede, S.E., Schroeder, J.R., Wang, Y., Wennberg, P.O., Zeng, L., 2020. Characterization, sources and reactivity of volatile organic compounds (VOCs) in Seoul and surrounding regions during KORUS-AQ. Elem. Sci. Anthr. 8, 37. https://doi.org/10.1525/elementa.434

Sakar, C., Sinha, V., Baerbel, S., Arnico, K.P., Maheswar, R., Lawrence, M.G., Source apportionment of NMVOCs in the Kathmandu Valley during the SusKat-ABC international field campaign using positive matrix factorization, Atmos. Chem and Phys., 17, 8129–8156, 7 https://doi.org/10.5194/acp-17-8129-2017, 2017

Tan, Z., Lu, K., Jiang, M., Su, R., Dong, H., Zeng, L., Xie, S., Tan, Q., Zhang, Y., 2018. Exploring ozone pollution in Chengdu, southwestern China: A case study from radical chemistry to O3-VOC-NOx sensitivity. Sci. Total Environ. 636, 775–786. https://doi.org/10.1016/j.scitotenv.2018.04.286

Tang, J.H., Chan, L.Y., Chan, C.Y., Li, Y.S., Chang, C.C., Liu, S.C., Wu, D., Li, Y.D., 2007. Characteristics and diurnal variations of NMHCs at urban, suburban, and rural sites in the Pearl River Delta and a remote site in South China. Atmos. Environ. 41, 8620–8632. https://doi.org/10.1016/j.atmosenv.2007.07.029

Thera, B., Dominutti, P., Colomb, A., Michoud, V., Doussin, J.-F., Beekmann, M., Dulac, F., Sartelet, K., Borbon, A., 2022. O 3 –NO y photochemistry in boundary layer polluted plumes: insights from the MEGAPOLI (Paris), ChArMEx/SAFMED (North West Mediterranean) and DACCIWA (southern West Africa) aircraft campaigns. Environ. Sci. Atmospheres. https://doi.org/10.1039/d1ea00093d

Varotsos, C.A., Mazei, Y., Saldaev, D., Efstathiou, M., Voronova, T., Xue, Y., 2021. Nowcasting of air pollution episodes in megacities: A case study for Athens, Greece. Atmospheric Pollut. Res. 12, 101099. https://doi.org/10.1016/j.apr.2021.101099

Vohra, K., Marais, E.A., Bloss, W.J., Schwartz, J., Mickley, L.J., Van Damme, M., Clarisse, L., Coheur, P.-F., 2022. Rapid rise in premature mortality due to anthropogenic air pollution in fast-growing tropical cities from 2005 to 2018. Sci. Adv. 8, eabm4435. https://doi.org/10.1126/sciadv.abm4435

Warneke, C., McKeen, S. a, Gouw, J.A. de, Goldan, P.D., Kuster, W.C., Holloway, J.S., Williams, E.J., Lerner, B.M., Parrish, D.D., Trainer, M., Fehsenfeld, F.C., Kato, S., Atlas, E.L.,

Baker, A., Blake, D.R., 2007. Determination of urban volatile organic compound emission ratios and comparison with an emissions database. J. Geophys. Res. 112, D10S47. https://doi.org/10.1029/2006JD007930

Warneke, C., Roberts, J.M., Veres, P., Gilman, J., Kuster, W.C., Burling, I., Yokelson, R., De Gouw, J.A., 2011. VOC identification and inter-comparison from laboratory biomass burning using PTR-MS and PIT-MS. Int. J. Mass Spectrom. 303, 6–14. https://doi.org/10.1016/j.ijms.2010.12.002

Warneke, C., Trainer, M., de Gouw, J.A., Parrish, D.D., Fahey, D.W., Ravishankara, A.R., Middlebrook, A.M., Brock, C.A., Roberts, J.M., Brown, S.S., Neuman, J.A., Lerner, B.M., Lack, D., Law, D., Hübler, G., Pollack, I., Sjostedt, S., Ryerson, T.B., Gilman, J.B., Liao, J., Holloway, J., Peischl, J., Nowak, J.B., Aikin, K.C., Min, K.-E., Washenfelder, R.A., Graus, M.G., Richardson, M., Markovic, M.Z., Wagner, N.L., Welti, A., Veres, P.R., Edwards, P., Schwarz, J.P., Gordon, T., Dube, W.P., McKeen, S.A., Brioude, J., Ahmadov, R., Bougiatioti, A., Lin, J.J., Nenes, A., Wolfe, G.M., Hanisco, T.F., Lee, B.H., Lopez-Hilfiker, F.D., Thornton, J.A., Keutsch, F.N., Kaiser, J., Mao, J., Hatch, C.D., 2016. Instrumentation and measurement strategy for the NOAA SENEX aircraftcampaign as part of the Southeast Atmosphere Study 2013. Atmospheric Meas. Tech. 9, 3063–3093. https://doi.org/10.5194/amt-9-3063-2016

Watson, J.G., Chow, J.C., Fujita, E.M., 2001. Review of volatile organic compound source apportionment by chemical mass balance. Atmos. Environ. 35, 1567–1584. https://doi.org/10.1016/S1352-2310(00)00461-1

WHO, 2018. Burden of disease from ambient air pollution for 2016, version 2. World Health Organization.

Wilde, S.E., Dominutti, P.A., Allen, G., Andrews, S.J., Bateson, P., Bauguitte, S.J.-B., Burton, R.R., Colfescu, I., France, J., Hopkins, J.R., Huang, L., Jones, A.E., Lachlan-Cope, T., Lee, J.D., Lewis, A.C., Mobbs, S.D., Weiss, A., Young, S., Purvis, R.M., 2021. Speciation

of VOC emissions related to offshore North Sea oil and gas production. Atmospheric Chem. Phys. 21, 3741–3762. https://doi.org/10.5194/acp-21-3741-2021

Wood, E.C., Herndon, S.C., Onasch, T.B., Kroll, J.H., Canagaratna, M.R., Kolb, C.E., Worsnop, D.R., Neuman, J.A., Seila, R., Zavala, M., Knighton, W.B., 2009. A case study of ozone production, nitrogen oxides, and the radical budget in Mexico City. Atmospheric Chem. Phys. 9, 2499–2516. https://doi.org/10.5194/acp-9-2499-2009

Wu, W., Zhao, B., Wang, S., Hao, J., 2017. Ozone and secondary organic aerosol formation potential from anthropogenic volatile organic compounds emissions in China. J. Environ. Sci. China 53, 224–237. https://doi.org/10.1016/j.jes.2016.03.025

Yang, X., Xue, L., Yao, L., Li, Q., Wen, L., Zhu, Y., Chen, T., Wang, X., Yang, L., Wang, T., Lee, S., Chen, J., Wang, W., 2017. Carbonyl compounds at Mount Tai in the North China Plain: Characteristics, sources, and effects on ozone formation. Atmospheric Res. 196, 53–61. https://doi.org/10.1016/j.atmosres.2017.06.005

Yu, D., Tan, Z., Lu, K., Ma, X., Li, X., Chen, S., Zhu, B., Lin, L., Li, Y., Qiu, P., Yang, X., Liu, Y., Wang, H., He, L., Huang, X., Zhang, Y., 2020. An explicit study of local ozone budget and NOx-VOCs sensitivity in Shenzhen China. Atmos. Environ. 224, 117304. https://doi.org/10.1016/j.atmosenv.2020.117304

Zannoni, N., Gros, V., Sarda Esteve, R., Kalogridis, C., Michoud, V., Dusanter, S., Sauvage, S., Locoge, N., Colomb, A., Bonsang, B., 2017. Summertime OH reactivity from a receptor coastal site in the Mediterranean Basin. Atmospheric Chem. Phys. 17, 12645–12658. https://doi.org/10.5194/acp-17-12645-2017

Zheng, J., Shao, M., Che, W., Zhang, L., Zhong, L., Zhang, Y., Streets, D., 2009. Speciated VOC Emission Inventory and Spatial Patterns of Ozone Formation Potential in the Pearl River Delta , China. Environ. Sci. Technol. 43, 8580–8586.

Table 1: Flights selected for this study. The mean of ozone and the total of measured VOC (TVOC) mixing ratios are also reported. For TVOC calculation, HCHO was not considered, and isoprene was not included during the SAFMED campaign flights.

Region	Flight N°	Date	Time (LT)	Ozone (ppbv)	Sector/Flight type	TVOC (ppbv)	
						Plume	Background
Paris area	25	1/7/2009	11:39-15:27	73.6	South-West Paris	31.7 ± 4.0	19.3 ± 6.7
	27	10/7/2009	11:08-14:58	39.3	East Paris	8.8 ± 0.9	7.8 ±1.0
	33	07/25/2009	11:02-16:47	31.1	East Paris	6.1 ± 0.9	6.2 ± 0.9
	36	07/29/2009	11:40-15:23	52.5	North Paris	15.2 ± 2.7	14.3 ± 1.6
North West Mediterranean	46	07/24/2013	12:49-14:58	63.7	Genova to Cagliari	10.5 ± 5.9	
	47	07/24/2013	16:46-18:14	63.7	Tyreman sea	9.5 ± 1.3	
	48	07/25/2013	15 :12-16 :56	63.9	Gulf of Genoa	13.1 ± 3.4	
	49	7/27/2013	11:08-13:07	57.8	Italy inland to Olbia	20 ± 1.6	
	51	7/30/2013	13:05-15:50	50.6	Gulf of Genoa	9.0 ± 0.7	
	52	8/1/2013	14 :48-17 :18	58.3	Genoa to Olbia	8.7 ± 0.7	
South West Africa	18	6/30/2016	12:36-16:10	30.4	City of Lomé, Biogenic surface and cloudy	32.5 ± 7.3	41.7 ± 8.4
	19	1/7/2016	10:22-13:49	34.4	Cloud, Accra city, Biogenic	12.6 ±4.0	12.7 ± 4.1
	23	7/5/2016	08:02-10:50	32.4	City of Lomé, Cloudy	15.4 ± 3.1	25.6 ± 10.9
	24	7/6/2016	07:08-10:50	30.5	Cities of Accra, Abidjan, Biogenic, Cloudy, Biomass Burning	12.4 ± 3.4	10.3 ± 3.1
	32	7/12/2016	13:38-16:59	37.4	Cloud, Accra city, Biogenic, Biomass Burning	5.9 ± 4.8	3.4 ± 1.4

Table 2: Statistical values of the average VOC mixing ratios (in ppb_v) inside the plumes during the MEGAPOLI, ChArMEX/SAFMED and DACCIWA campaigns.

VOC	Paris (MEGAPOLI)					North-West Mediterranean Basin (SAFMED)					South West Africa (DACCIWA)				
	Min	Max	Med	Mean	Std	Min	Max	Med	Mean	Std	Min	Max	Med	Mean	Std
benzene	0.004	0.430	0.110	0.130	0.090	0.001	0.530	0.110	0.120	0.080	0.010	2.380	0.240	0.430	0.480
toluene	0.007	1.450	0.280	0.350	0.250	0.002	0.490	0.100	0.120	0.080	0.010	1.320	0.320	0.410	0.320
C_8 aromatics	0.000	0.970	0.200	0.220	0.150	0.000	1.030	0.110	0.150	0.130	0.010	0.740	0.130	0.190	0.160
C_9 aromatics	0.005	0.490	0.100	0.110	0.080	0.001	2.900	0.540	0.610	0.460	0.010	0.930	0.140	0.180	0.150
isoprene	0.030	7.990	0.970	1.550	2.140	n.m.	n.m.	n.m.	n.m.	n.m.	0.080	8.000	1.730	2.360	1.830
MACR +MVK	0.000	1.390	0.320	0.450	0.380	0.003	4.340	1.160	1.480	0.930	0.010	7.130	0.640	0.890	0.950
MEK	0.020	1.480	0.460	0.540	0.390	0.020	1.680	0.610	0.730	0.360	0.010	2.230	0.570	0.720	0.530
monoterpenes	0.010	0.560	0.170	0.200	0.150	0.001	1.000	0.250	0.300	0.180	0.010	1.010	0.150	0.230	0.190
methanol	0.860	7.660	3.260	3.970	1.900	0.010	3.950	2.070	2.010	0.880	0.040	7.160	1.440	1.820	1.430
acetaldehyde	0.010	6.100	0.540	1.490	1.850	0.010	3.200	0.740	1.040	0.750	0.010	33.700	2.820	6.770	7.500
acetone	0.490	7.990	2.500	2.810	1.930	0.210	14.320	3.040	3.080	1.350	0.020	11.030	1.700	2.800	2.840
formaldehyde	n.m.	n.m.	n.m.	n.m.	n.m.	2.400	5.000	3.300	3.600	0.800	0.650	11.700	3.490	3.520	1.970

n.m. : non measured concentrations

Table 3: Production or decay rates in ppt_v VOC.ppb_v^{-1} CO per hour of AVOC and OVOC in the Paris plumes during MEGAPOLI. Rates are the slope of a least-square linear fit. Grey values highlight the production of VOC (positive slope), and black values highlight the decay of VOC (negative slope). Italics indicate R^2 coefficients < 0.50.

VOC	Flight #25 slope ± σ	R^2	Flight #27 slope ± σ	R^2	Flight #33 slope ± σ	R^2	Flight #36 slope ± σ	R^2
Benzene	-1.05 ± 0.59	R² = 0.76	nd	nd	nd	nd	*-3.49 ± 1.42*	*R² = 0.21*
Toluene	-0.71 ± 0.70	R² = 0.51	-0.57 ± 0.15	R² = 0.93	-0.81 ± 0.33	R² = 0.85	*-1.80 ± 2.07*	*R² = 0.27*
C8-aromatics	-1.37 ± 0.66	R² = 0.81	-1.62 ± 0.42	R² = 0.94	-0.87 ± 0.57	R² = 0.54	-3.19 ± 0.89	R² = 0.86
C9-aromatics	nd	nd	nd	nd	nd	nd	-0.31 ± 0.18	R² = 0.60
Methanol	11.9 ± 3.25	R² = 0.93	*0.26 ± 2.12*	*R² = 0.01*	*17.9 ± 6.14*	*R² = 0.19*	nd	nd
acetone	3.50 ± 0.44	R² = 0.98	*1.21 ± 1.02*	*R² = 0.41*	11.8 ± 4.71	R² = 0.75	*-1.85 ± 3.25*	*R² = 0.13*
acetaldehyde	*-1.31 ± 4.26*	*R² = 0.08*	*2.01 ± 2.64*	*R² = 0.22*	18.02 ± 2.13	R² = 0.97	-7.76 ± 5.31	R² = 0.52
MACR+MVK	-4.37 ± 1.65	R² = 0.87	0.87 ± 0.52	R² = 0.58	*0.94 ± 0.85*	*R² = 0.38*	-2.80 ± 1.53	R² = 0.62
MEK	-1.38 ± 0.21	R² = 0.97	*1.04 ± 0.76*	*R² = 0.48*	4.37 ± 0.79	R² = 0.93	*-3.89 ± 3.19*	*R² = 0.42*

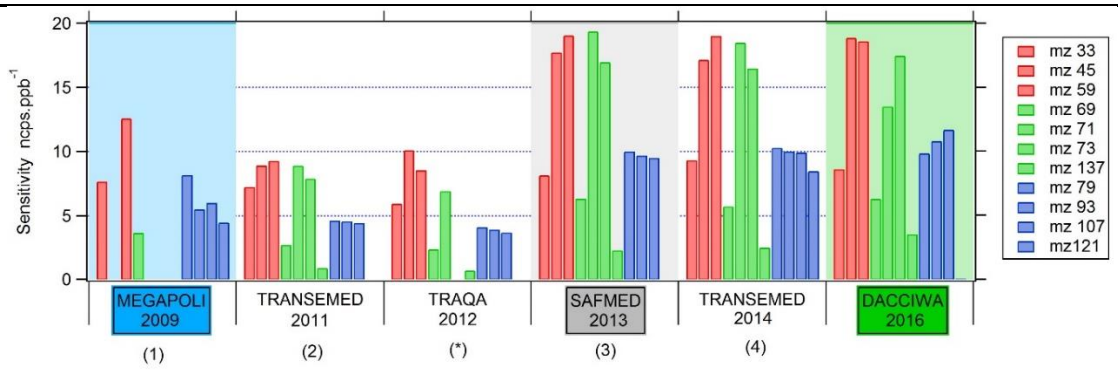

Figure 1: Comparison of the Q-PTR-MS normalised sensitivities during aircraft and ground-based campaigns between 2009 and 2016. The values are from various publications indicated by the numbers on parenthesis on the x-axis: (1) Borbon et al. (2013); (2) Borbon et al. (2023); (3) Freney et al. (2014); (4) Thera et al. (2019); (*) unpublished results from our group during the TRAQA aircraft campaign (Di Biagio et al., 2015).

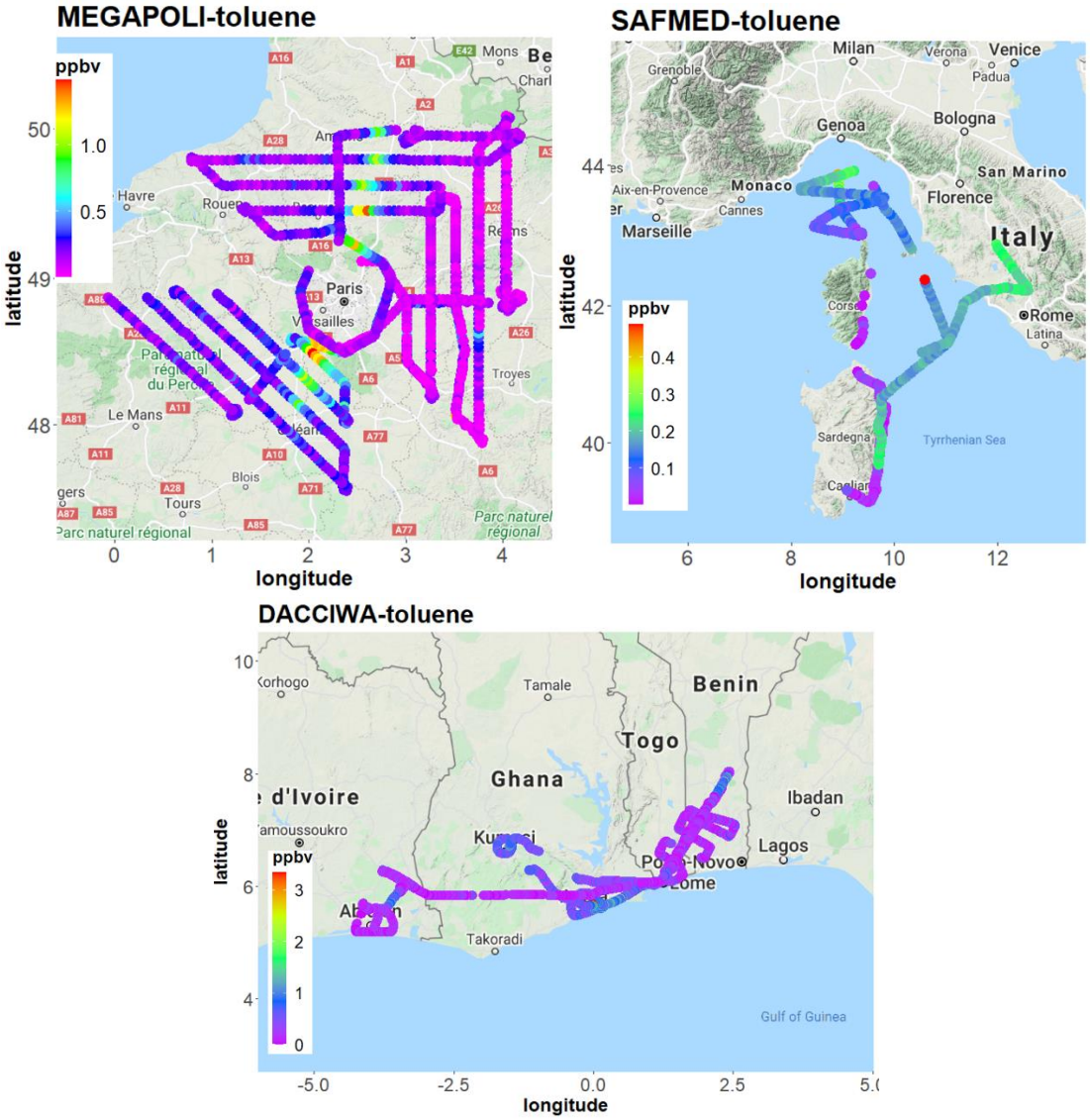

Figure 2: Trajectories of selected flights for MEGAPOLI, ChArMEx/SAFMED and DACCIWA aircraft campaigns colour-coded by toluene mixing ratios (in ppb_v) within the boundary layer.

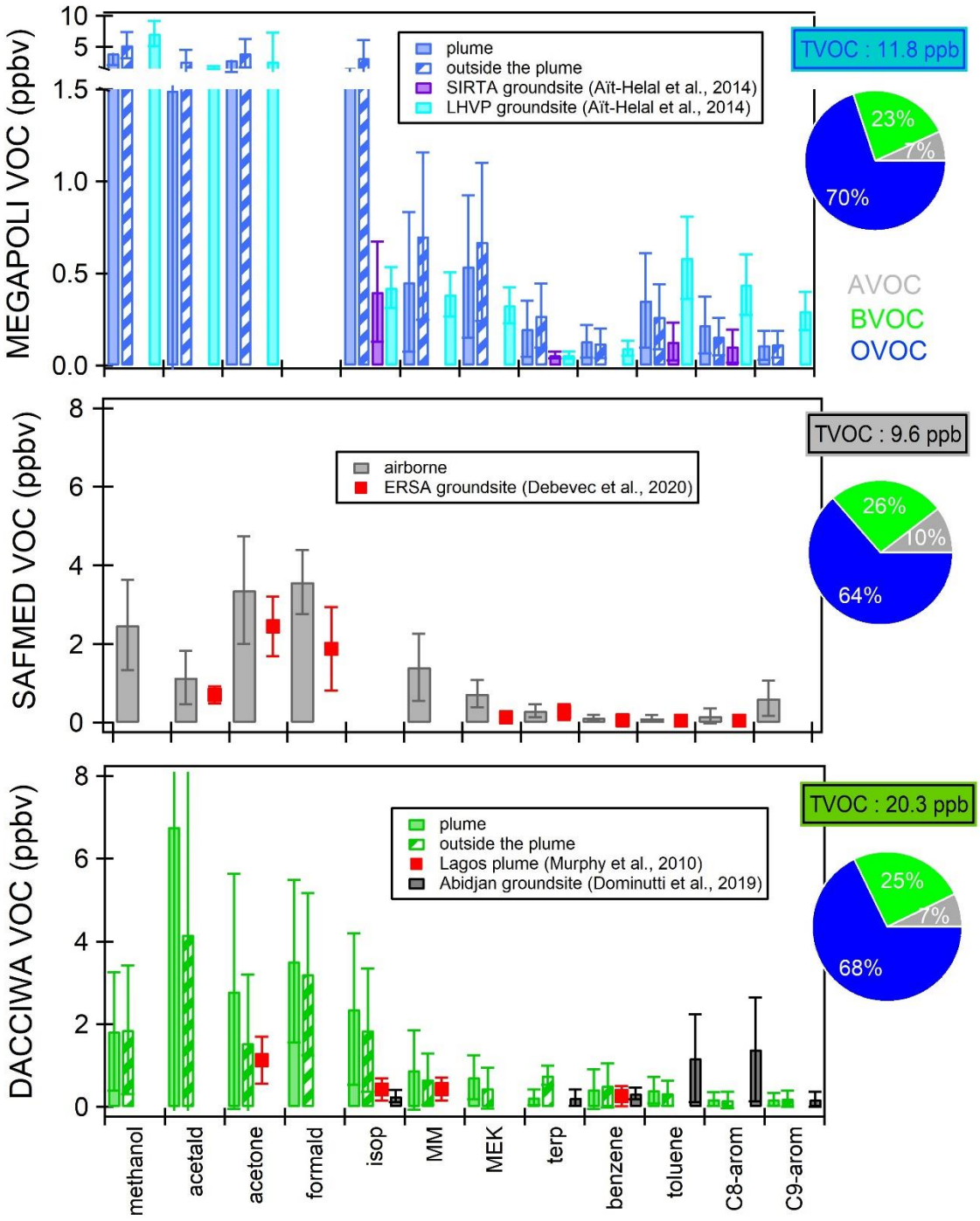

Figure 3: Average mixing ratios and standard deviations of VOCs inside and outside plumes during the target campaigns except SAFMED. Compounds: acetald: acetaldehyde, acetone, formald: formaldehyde, isop: isoprene, MM: MACR+MVK, 7: MEK, terp: monoterpenes, C8-arom: C_8 aromatics, C9-arom: C_9 aromatics. The pie charts represent the average contributions of AVOC, BVOC and OVOC (formaldehyde is excluded) to the total VOC in ppb during each campaign.

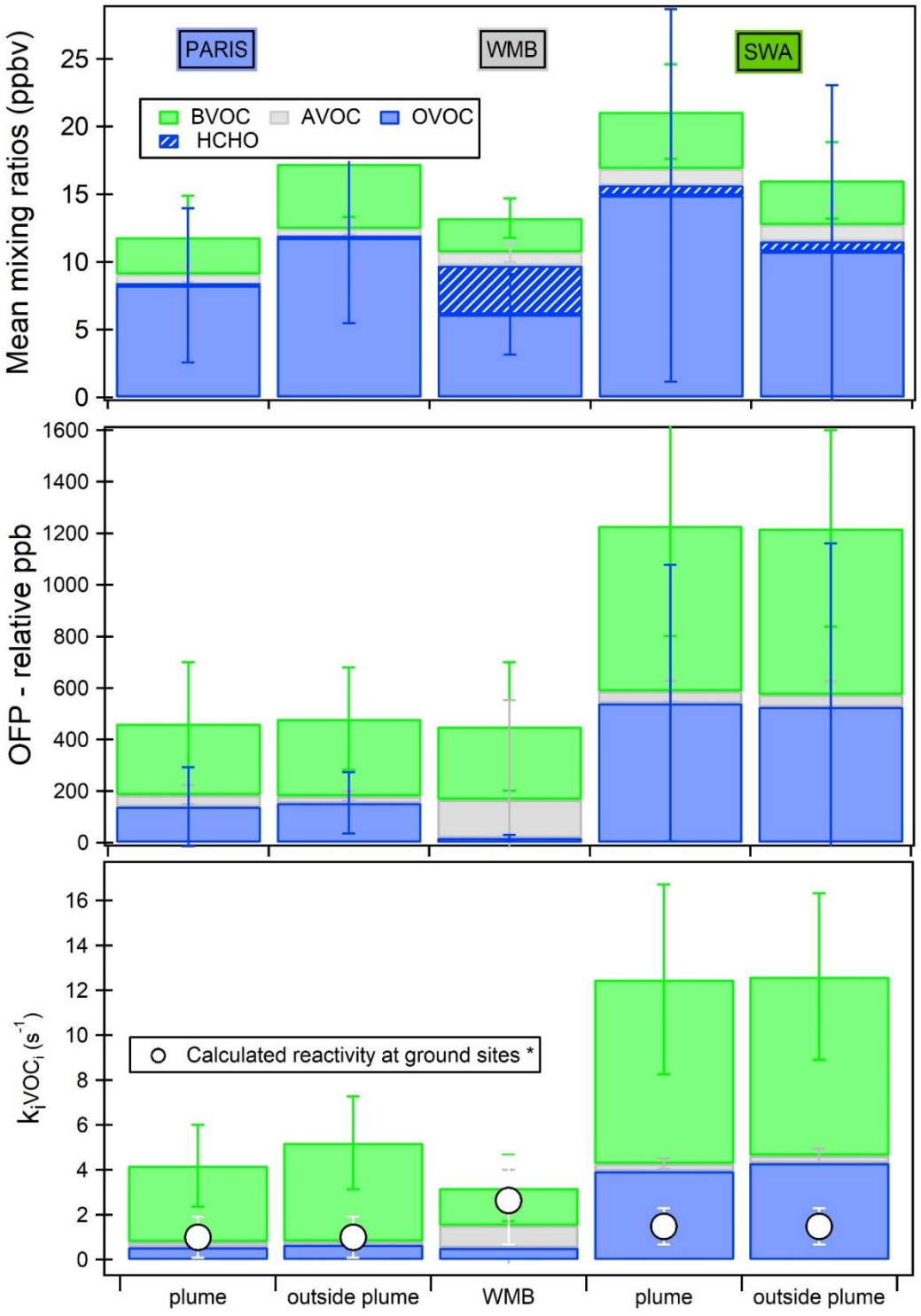

Figure 4: ·OH radical loss rate (kiVOCi) and ozone formation potential (OFP relative ppb) for BVOC, OVOC and AVOC during MEGAPOLI, SAFMED and DACCIWA campaigns. Formaldehyde was only measured during SAFMED and DACCIWA campaigns. White dots represent the ·OH radical loss rate (kiVOCi) obtained from the measurements performed at ground-based campaigns in Paris (urban site, Baudic et al., 2016), Ersa, Cape Corsica (remote site, Michoud et al., 2017), and Abidjan (urban sites, Dominutti et al., 2019, no OVOC data available).

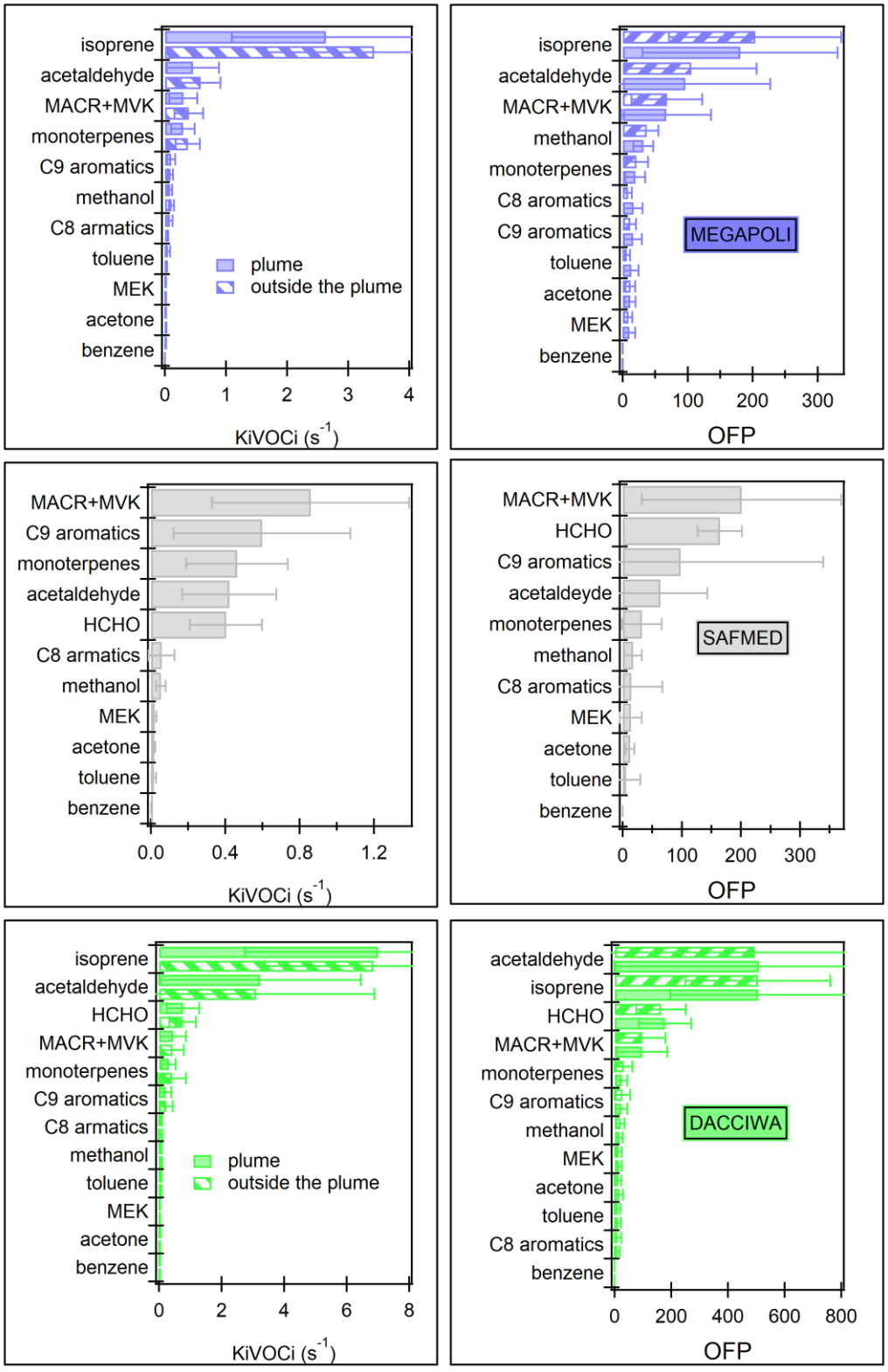

Figure 5: Top VOC reactivities observed inside (shaded bars) and outside (striped bars) plumes during each campaign in decreasing contribution order.

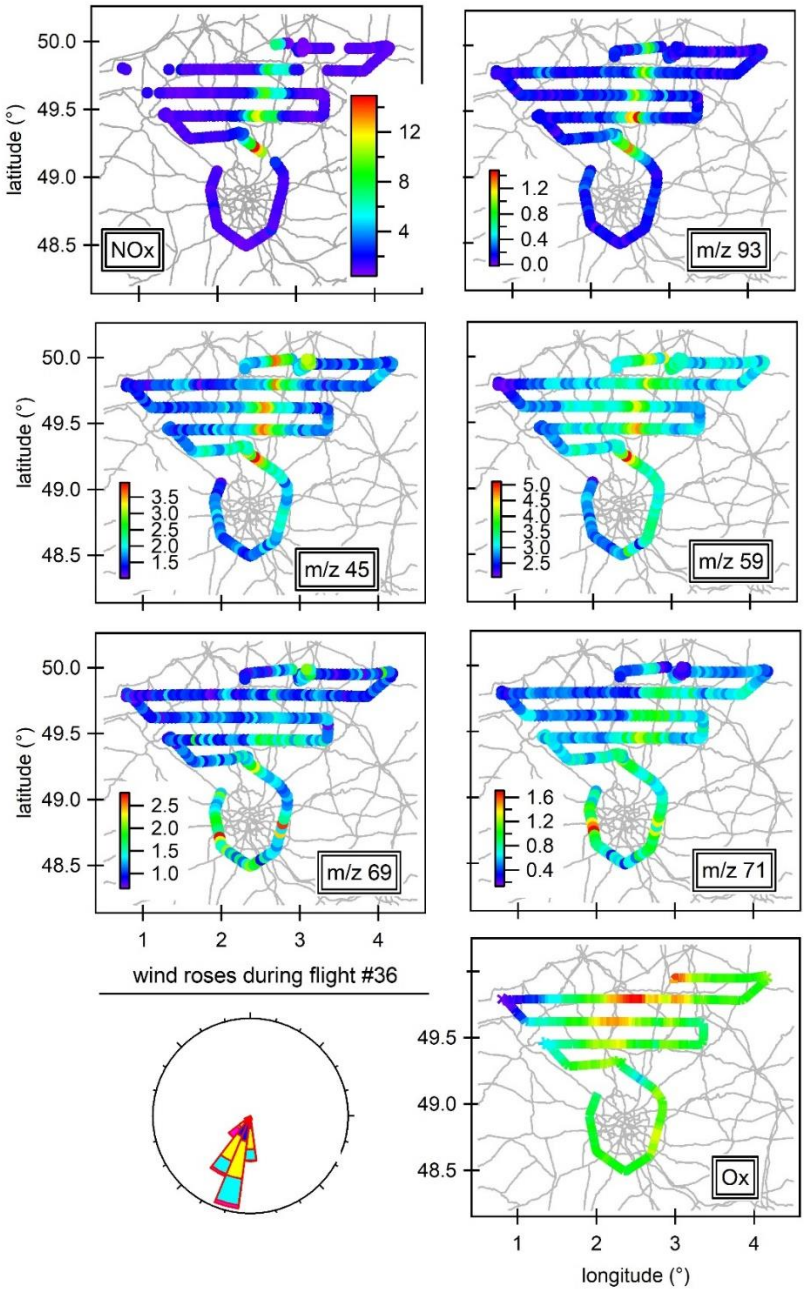

Figure 6: ATR-42 trajectory color-coded by trace gas mixing ratios (ppb_v) during MEGAPOLI flight 36. The wind roses in the lower left-hand panel indicates southern.

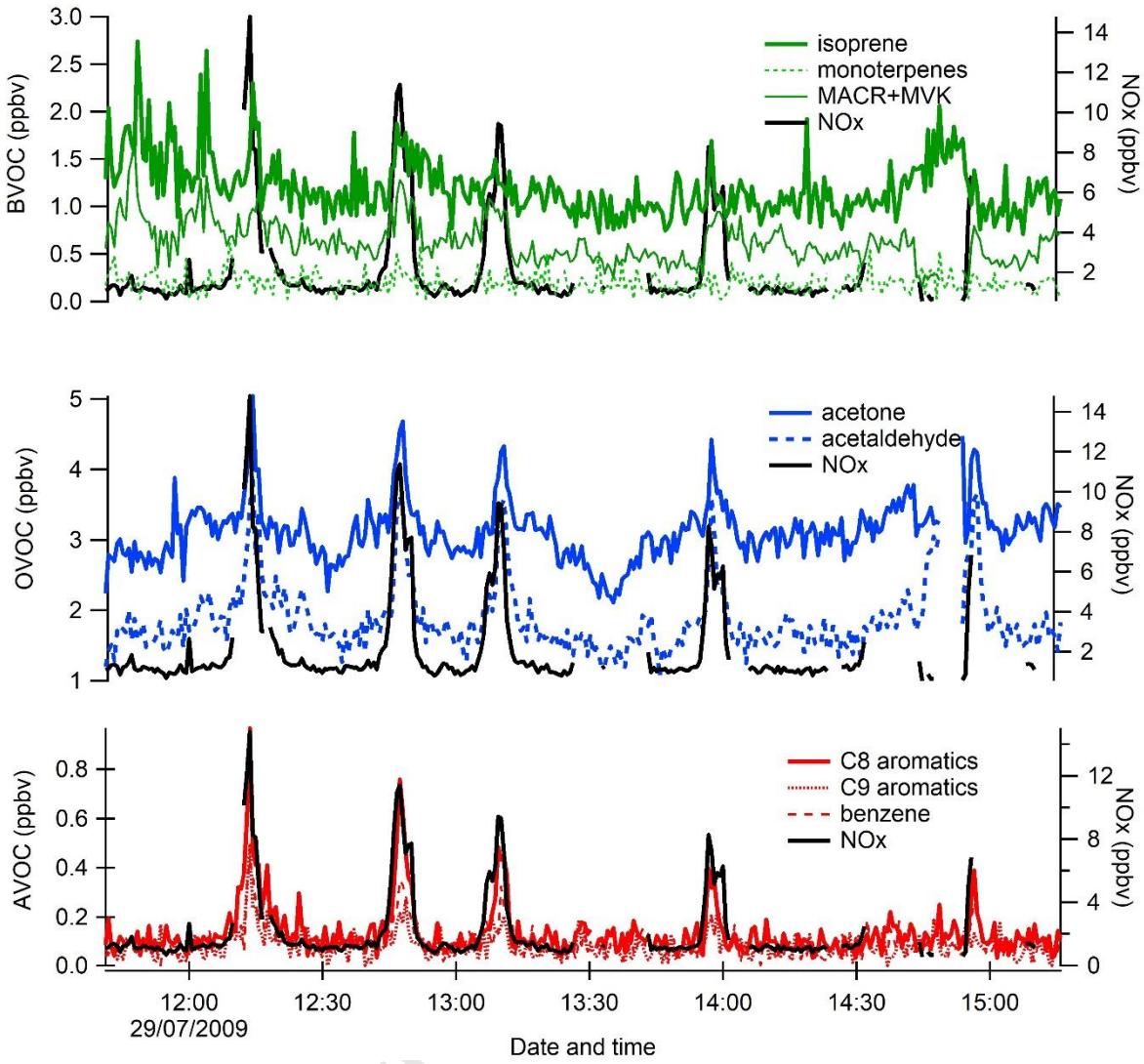

Figure 7: Time series (UTC Time) of NOx, AVOC, BVOC and OVOC mixing ratios during the exploration of the boundary layer of the MEGAPOLI flight 36.

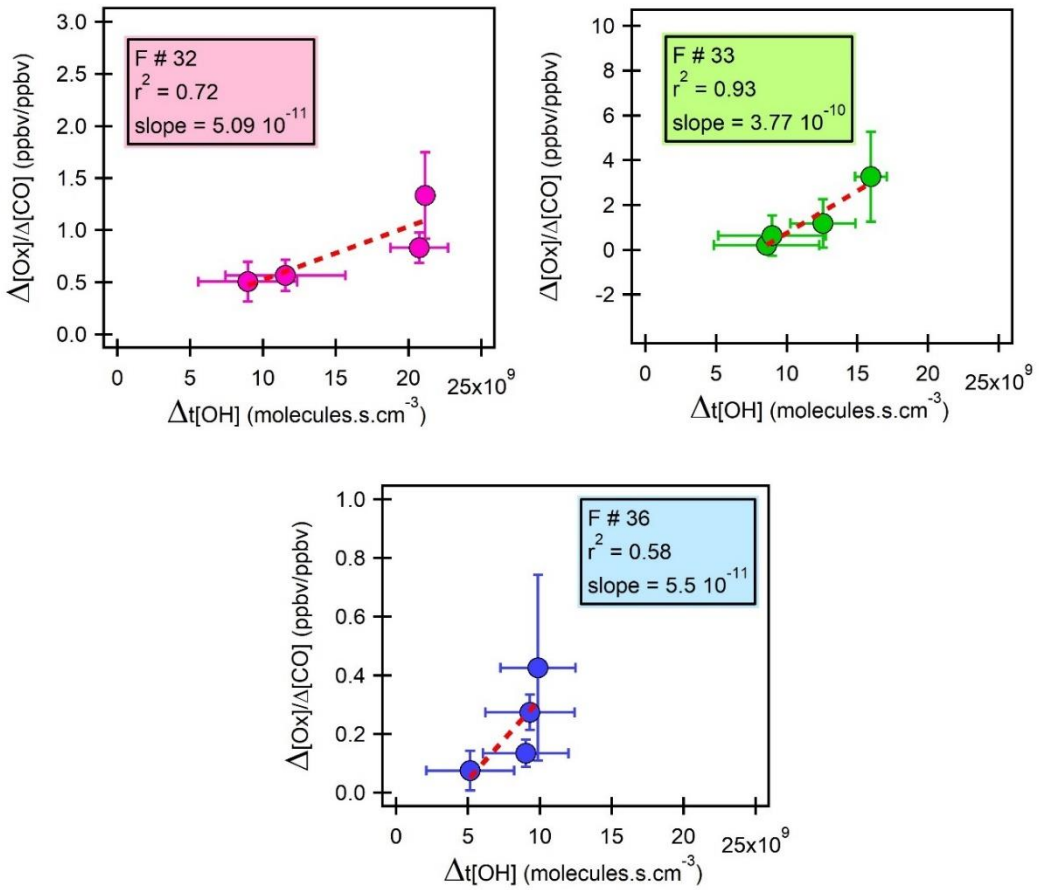

Figure 8: Scatterplots of ΔOx divided by ΔCO versus the cumulative ·OH exposure (ΔOH) for Paris plume during flights 32, 33, and 36 of the MEGAPOLI campaign.

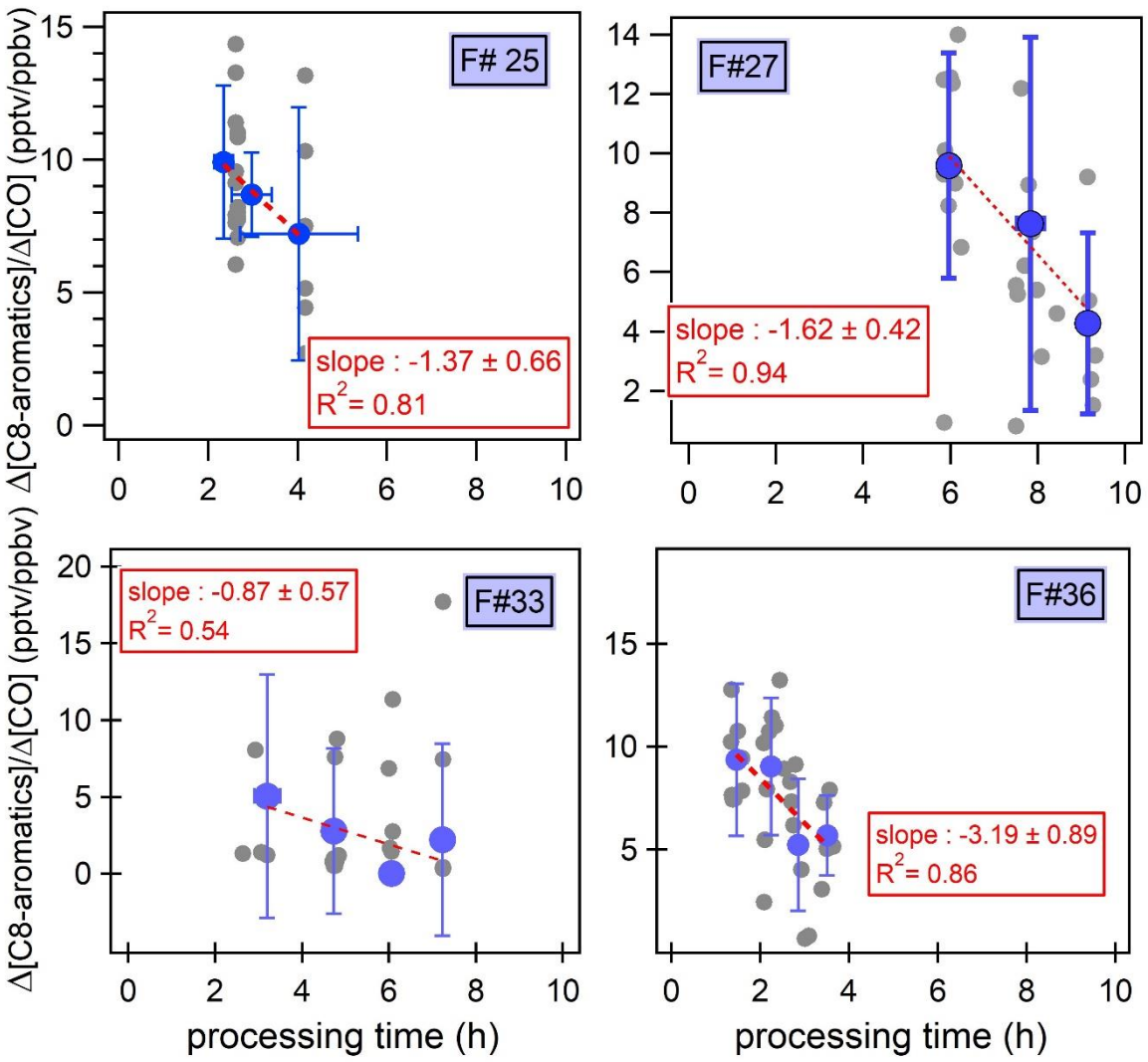

Figure 9: Scatterplot of C_8-aromatics-to-CO as a function of the processing time inside the Paris plume during flights 25, 27, 33 and 36 of MEGAPOLI. Blue dots represent the mean values and the standard deviation of the ΔVOC/ΔCO calculated for each plume transect. Red dashed lines represent the slope of the mean values.

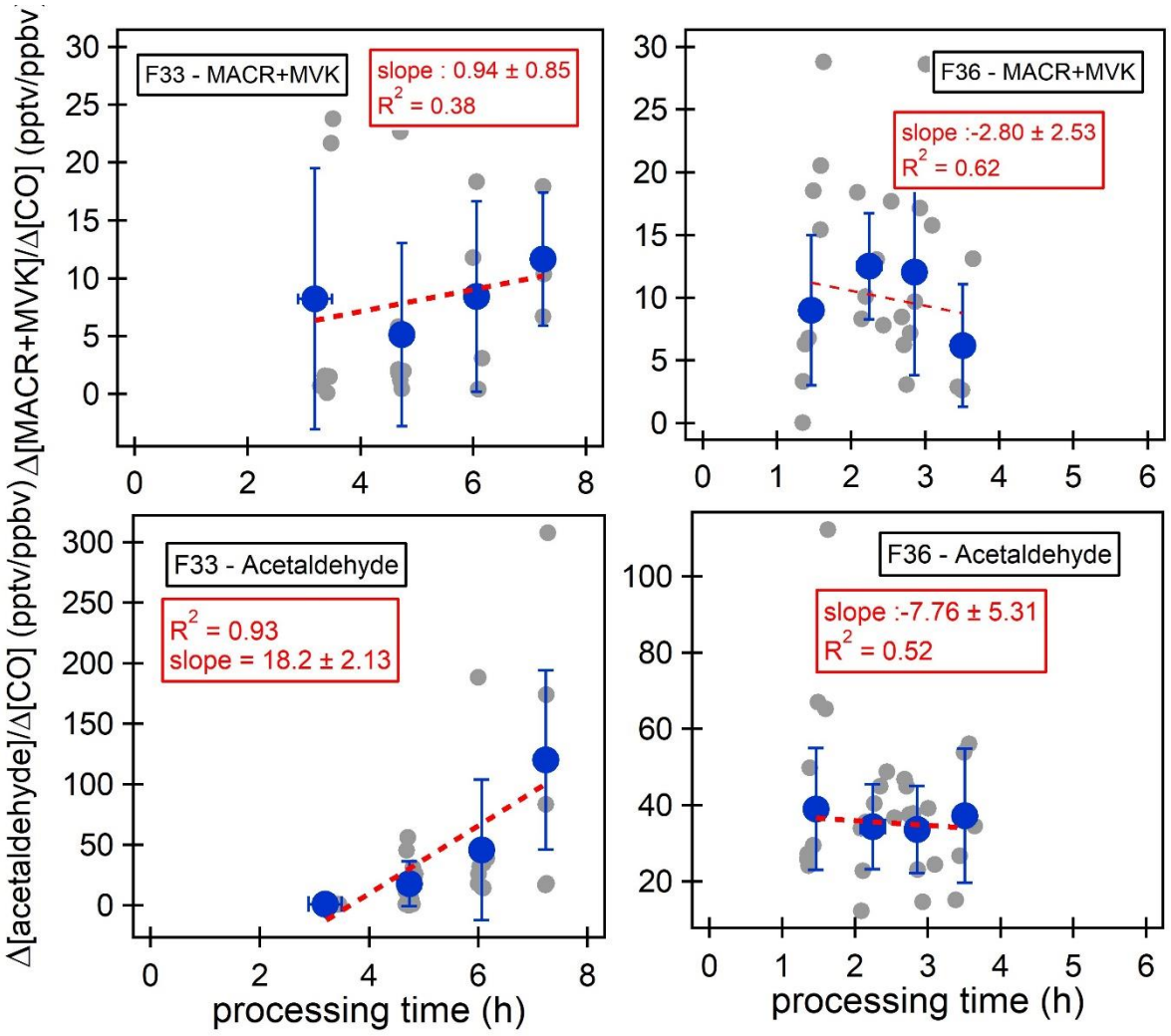

Figure 10: Scatterplots of ΔOVOC-to-ΔCO vs. the processing time inside the Paris plume observed during flights 33 and 36 of MEGAPOLI.

Declaration of interests

☐The authors declare that they have no known competing financial interests or personal relationships that could have appeared to influence the work reported in this paper.

☒The authors declare the following financial interests/personal relationships which may be considered as potential competing interests:

Agnes Borbon reports financial support was provided by European Commission. Agnes Borbon reports financial support was provided by French National Research Agency. Agnes Borbon reports financial support was provided by National Centre for Scientific Research. If there are other authors, they declare that they have no known competing financial interests or personal relationships that could have appeared to influence the work reported in this paper.

Graphical abstract

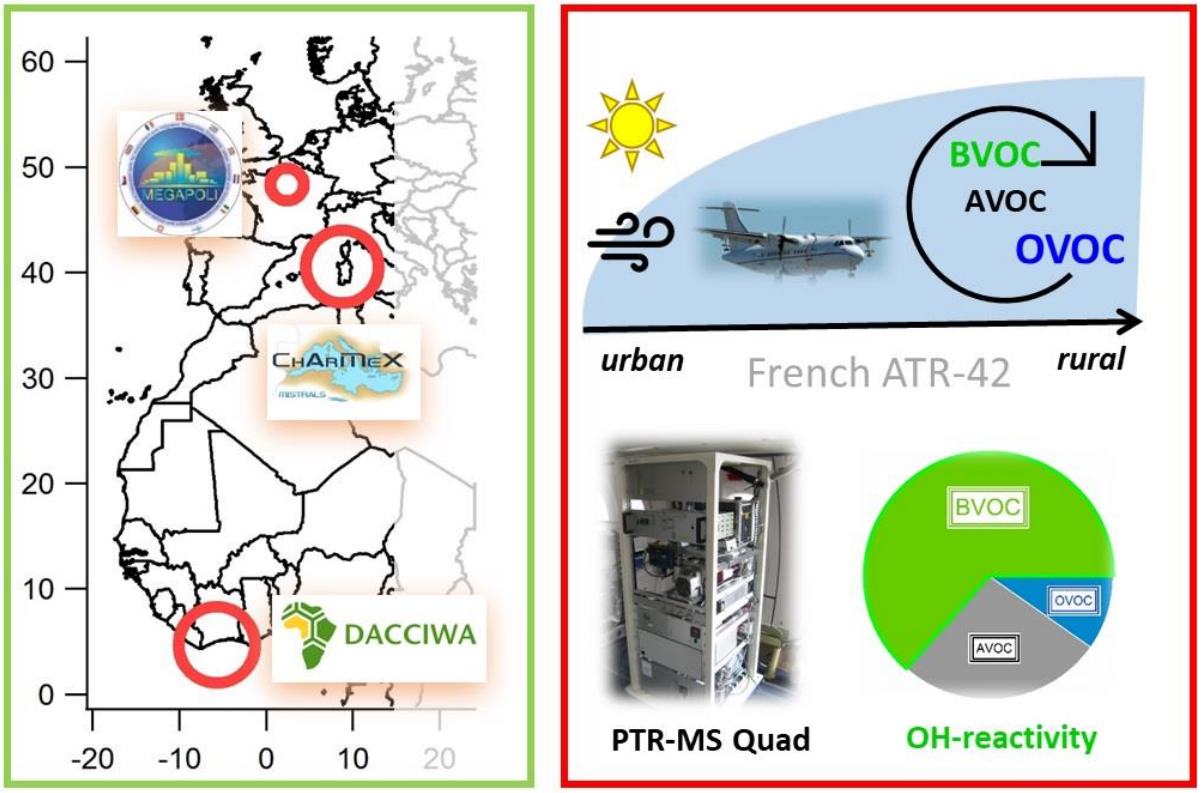

Highlights

- The VOC composition of European, South-West Africa and Mediterranean plumes are analysed
- Oxygenated VOC dominate the composition of the plumes regardless of the location
- The OH-reactivity of the plumes is dominated by biogenic VOC regardless of the location
- The decay rate of AVOC and/or the secondary production of OVOC is demonstrated and quantified